ELEMENTA
Science of the Anthropocene

A characterization of Arctic aerosols on the basis of aerosol optical depth and black carbon measurements

R. S. Stone[1,2] • S. Sharma[3] • A. Herber[4*] • K. Eleftheriadis[5] • D. W. Nelson[2]

[1]Cooperative Institute for Research in Environmental Sciences, University of Colorado Boulder, Boulder, Colorado, United States
[2]NOAA Earth Systems Research Laboratory, Boulder, Colorado, United States
[3]Environment Canada, Downsview, Ontario, Canada
[4]Alfred Wegener Institute Helmholtz Centre for Polar and Marine Research, Bremerhaven, Germany
[5]Environmental Radioactivity Laboratory, National Center for Scientific Research Demokritos, Athens, Greece
*ANDREAS.HERBER@awi.de

Abstract

Aerosols, transported from distant source regions, influence the Arctic surface radiation budget. When deposited on snow and ice, carbonaceous particles can reduce the surface albedo, which accelerates melting, leading to a temperature-albedo feedback that amplifies Arctic warming. Black carbon (BC), in particular, has been implicated as a major warming agent at high latitudes. BC and co-emitted aerosols in the atmosphere, however, attenuate sunlight and radiatively cool the surface. Warming by soot deposition and cooling by atmospheric aerosols are referred to as "darkening" and "dimming" effects, respectively. In this study, climatologies of spectral aerosol optical depth AOD (2001–2011) and Equivalent BC (EBC) (1989–2011) from three Arctic observatories and from a number of aircraft campaigns are used to characterize Arctic aerosols. Since the 1980s, concentrations of BC in the Arctic have decreased by more than 50% at ground stations where in situ observations are made. AOD has increased slightly during the past decade, with variations attributed to changing emission inventories and source strengths of natural aerosols, including biomass smoke and volcanic aerosol, further influenced by deposition rates and airflow patterns.

Domain Editor-in-Chief
Detlev Helmig, University of Colorado Boulder

Associate Editor
Jan W. Bottenheim, Environment Canada, Canada

Knowledge Domain
Atmospheric Science

Article Type
Research Article

Received: August 30, 2013
Accepted: April 29, 2014
Published: June 10, 2014

Introduction

The Arctic was once thought to be a pristine environment. As early as 1870, however, Nordenskiöld (1883) found anecdotal evidence that the Arctic was being contaminated by pollutants transported from lower latitudes (e.g., Stohl et al., 2006; Hirdman et al., 2009). During the 1950s, U.S. pilots on reconnaissance flights into the Arctic reported seeing layers of pollutants (Mitchell, 1957). The phenomenon was thereafter referred to as Arctic haze, thought to be composed of soot, dust and sulfates emitted by industrial complexes located in Eurasia, transported into the Arctic during winter and spring (Shaw, 1983; 1995). Haze is known to perturb the Arctic surface-atmosphere radiation balance (e.g., Shaw and Stamnes, 1980; Blanchet, 1989). The Arctic presents particular challenges when assessing aerosol impacts due to large variations in aerosol concentration, and their varying chemical, physical and optical properties. The task is further complicated by dramatic changes in solar geometry and surface albedo that occur seasonally at high latitudes. While not a focus here, aerosols also interact with clouds to affect their microphysical and radiative properties (Twomey, 1977; Kaufman and Fraser, 1997), further modulating the radiation budget of the region.

In recent years, there has been much focus on the role of black carbon (BC), also referred to as soot or light absorbing carbon as a warming agent in the Arctic (e.g., Bond et al., 2013). BC is known to warm the atmosphere (e.g., Ramanathan and Carmichael, 2008; references therein) by absorbing solar radiation. Absorption by atmospheric BC also attenuates sunlight, contributing to 'dimming' by aerosols in general. When deposited on snow/ice, BC also absorbs radiation to reduce the surface albedo, a process referred to

as 'darkening' (e.g., Flanner, 2013; Flanner et al., 2007; Clarke and Noone, 2007). Such studies suggest that this darkening effect has contributed to the decline in Arctic sea ice (Stroeve et al., 2011). The simulations made by Flanner et al. (2007) show that darkening of the snow/ice by BC may have produced a warming at the surface in the Arctic of 0.5 to 1°C. Earlier snow or ice melt, in turn, leads to further warming of the atmosphere through an albedo feedback, thus increasing the "efficacy" of soot deposited on snow (Flanner et al., 2007). Stone et al. (2002; Table 2) present an empirical analysis of the albedo feedback caused by earlier snowmelt in the vicinity of Barrow, Alaska. They found that the radiative perturbation resulting from an earlier melt, by ≈ two weeks, increased the annual net energy budget by ≈ 2 Wm^{-2}, and over the summer season by as much as 14%. Partly in response to a two week advance in the melt date, June temperatures were about 1°C warmer on average, evidence of a temperature-albedo feedback. That study and a subsequent analysis by Stone et al. (2005), however, attribute variability in the date of snowmelt at Barrow to changes in regional circulation patterns, not to darkening of snow by BC deposition.

Despite collective efforts by many investigators, there remain large uncertainties in quantifying the radiative effects of atmospheric aerosols (IPCC, 2007). This is especially true in the Arctic, where not only the magnitude but also the sign of the surface forcing may vary. The darkening of snow and ice by soot is claimed to be a major contributor to recent Arctic warming. Past studies (e.g., Hansen and Nazarenko, 2004; Flanner et al., 2007; Quinn et al., 2007) suggest that the darkening effect of BC is greater than the cooling effect of reflective particles co-emitted with BC. On this basis, UNEP (2011) reports that reduction of BC and other short-lived climate pollutants (SLCPs) "would slow the projected warming in the Arctic by about 0.7°C in 2040 …". In response to these concerns, attempts to mitigate the release of SLCPs are underway, in part by "The Climate and Clean Air Coalition to Reduce Short-Lived Climate Pollutants" (http://www.state.gov/r/pa/prs/ps/2012/02/184055.htm). The goal of this coalition is to simultaneously reduce the health risks associated with pollutants, including BC and to slow global warming. Related to climate, they state the following: "reducing black carbon is particularly important to address climate change in snow- and ice-covered regions such as the Arctic…." It is therefore important to understand the relative impacts of dimming by atmospheric aerosols versus the darkening effect of BC deposited on snow and ice.

The deposition of BC on snow across the Arctic is highly variable (Doherty et al., 2010), depending on distance from source regions, deposition velocity and the time of year. Table 2 of Doherty et al. (2010) lists median values of BC concentration from snow and ice samples collected during 1998 and 2005–2009, by region. Median concentrations measured in the central Arctic were found to be much lower (~ 7 ng g^{-1}) than those close to emission sources in Russia (27-34 ± 46 ng g^{-1}). The lowest concentrations (~ 3 ng g^{-1}) were measured on the Greenland Ice Sheet at elevations above 2000 m, and thought to be representative of the free troposphere of that region. During the Surface Heat Budget of the Arctic Ocean (SHEBA) campaign (1998) Grenfell et al. (2002) measured average background concentrations of < 5 ngC/g in snow over sea ice. Such concentrations do not result in measurable decreases in surface albedo. A study by Hadley and Kirchstetter (2012) presents evidence from laboratory experiments showing responses of snow albedo to changes in concentrations of black carbon < 200 ppb (equivalent to 200 ng g^{-1}). Another study, however, found that sea ice albedo "is surprisingly unresponsive" to BC concentrations < 100 ng g^{-1} (Marks and King, 2013) and that overlying snow of < 5 cm depth substantially masks any change in surface albedo. Warren and Wiscombe (1980) estimate that when concentrations reach 15 ng g^{-1}, a 1% decrease in albedo will result at the wavelength of 500 nm, but snow surveys indicate that over most of the Arctic, current concentrations are significantly lower than 15 ng g^{-1} (Grenfell et al., 2002; Doherty et al., 2010). At shorter and longer wavelengths, the darkening effect is diminished significantly. Such small decreases in broadband albedo due to darkening by BC are not easily resolved using conventional radiometers because natural variations in snow albedo are on the order of a few percent, day-to-day (Stone et al., 1996). While the methodology to measure BC concentrations in snow is refined and accurate data are being obtained (Brandt et al., 2011), there remains the question of representativeness of samples collected. Samples collected vary on micro-scales and depend on depth and timing relative to deposition. Post-depositional processes (metamorphism) tend to move particles through the snow pack (Brandt et al., 2011). Although a large numbers of snow samples have been collected to represent regional distributions of BC in the Arctic, there remain uncertainties associated with assessments. Snow surveys are limited by difficult access to remote regions of the Arctic and are performed very infrequently. Time series of BC concentration are lacking and therefore it is difficult to perform meaningful trend analyses.

The darkening effect of soot in snow is most significant after the onset of melt in late spring at high northern latitudes. On sea ice, the impact occurs later in summer, after snow melt exposes bare ice (Marks and King, 2013). In both instances, the effects are confined to the period of melt, which is typically on the order of weeks during the annual cycle (Stone et al., 2002). During melt, soot particles tend to coagulate, possibly within growing snow grains and accumulate at the surface (Flanner et al., 2007). Snow/ice darkening will peak as the melt proceeds, accelerating but then quickly diminishing as the snow or ice disappears. Therefore, the warming effects of BC (and other absorbing particles in ice/snow) compete with the cooling effect of atmospheric aerosols differentially as the season progresses, depending on the relative burden of aerosols aloft and deposited at the surface.

Aerosol optical depth (AOD) is a measure of the total extinction (omni-directional scattering + absorption) of sunlight as it passes through the atmosphere. Therefore, surface cooling due to the attenuation of sunlight varies with AOD, which is being monitored with good accuracy at a number of Polar stations (Mazzola et al., 2011; references therein). When measured in conjunction with components of the surface radiation budget (SRB), it is possible to derive values of the direct radiative forcing efficiency (RFE) of various Arctic aerosols (e.g., Stone et al., 2007; 2008).

In the paper, we first provide an overview of how aerosols are transported to the Arctic from source regions. Dominant flow regimes are described. Next, representative AOD climatologies are presented for three Arctic climate observatories; Barrow, Alaska (BRW), Alert, Canada (ALT) and Ny-Ålesund, Svalbard (NYA). Monthly and year-to-year variations and trends in AOD and derived spectral parameters are presented. Corresponding, in situ measurements of equivalent black carbon (EBC) are similarly analyzed, updating the analysis of Sharma et al. (2004; 2006; 2013); and a compilation of BC data collected by aircraft (e.g., Schnell, 1984; Schnell et al., 1989; Skouratov, 1997; Yamanouchi et al., 2005; Brock et al., 2011; Warneke et al., 2010; Stone et al., 2010; Matsui et al. 2011) are used to evaluate BC concentrations within the troposphere. The profiles are used to evaluate variations in atmospheric BC over time. Note that, subsequently, specific definitions of EBC versus BC will be given, with reference to Appendix I.

Transport of aerosols into the Arctic

Figure 1 illustrates how aerosols from lower latitudes are, on average, transported to the Arctic during the winter/spring months. Fig. 1(a) is derived from gridded 850 mb geopotential height fields for years 2001–2011 extracted from NCEP/NCAR Reanalysis data; (http://www.esrl.noaa.gov/psd/data/gridded/reanalysis). The three observatories, BRW (B), ALT (A) and NYA (N), are indicated. Large-scale, planetary wave patterns determine flow to and within the Arctic, with circulation around quasi-persistent action centers; designated here as the Siberian High (SH), Aleutian Low (AL), Beaufort Anticyclone (BA), North American High (NAH), Icelandic Low (IL) and Central Arctic Low (CAL), or Arctic vortex. A High also persists over Greenland (GH). The arrows are drawn schematically to represent the 850 mb vector winds that circulate around the high and low pressure centers. BRW, ALT and NYA are impacted by different types of aerosol depending on pathways established by synoptic scale circulation patterns. The station AOD climatologies differ in accordance with source-receptor relationships, wherein coupling of adjacent pressure centers tend to favor certain flow patterns. For example, the coupling of the SH and Arctic vortex favors the transport of pollutants (Arctic haze) flowing eastward from Asia into the Arctic. Emissions, released within the SH, accumulate under stable atmospheric conditions and circulate north and east along its northern boundary. In the presence of sunlight, photochemical reactions may modify the aerosol chemical composition and thus aerosol properties. Elemental carbon mass, however, is conserved during transport because removal through dry or wet deposition is inhibited along isentropic surfaces (Raatz, 1989). Hirdman et al. (2009) provide a comprehensive analysis of the dispersion of pollutants from source regions to BRW, ALT and NYA (Zeppelin station), with a particular focus on EBC. They found that emissions within the Arctic and from high-latitude Eurasia were primary sources. Such was the case during April 2009 (Stone et al., 2010). Aerosols that survive long-range transport accumulate within the vortex over time and circulate for days to weeks (Quinn et al., 2007). As the vortex evolves and shifts position, other parts of the Arctic are affected. NYA appears most influenced by flow from the north, and is otherwise in a more pristine location. Aerosol outflow from North America tends to pass south of NYA. At an elevation of 464 m, the sampling site at NYA is often in the free troposphere where the influence of boundary layer aerosols is minimal. At other times, NYA experiences incursions of aerosol from Eurasia. Treffeisen et al., (2007) present a good example, documenting the flow of smoke from western Russia to NYA in May 2006. Described as atypical, the coupling of the IL and a High over Eastern Europe favored flow directly from the fire zone. More typical flow of Arctic haze to NYA during March 2008 is described by Stock et al. (2012). In that case, the coupling of the IL and SH favored the transport of pollutants into the central Arctic that were then advected southward to NYA. Long-term (~8 yr) Potential Source Contribution Function analysis by Eleftheriadis et al. (2009) indicated that high BC concentrations observed at Zeppelin station (NYA) were mainly influenced by source regions in northern and central Russia.

ALT is also influenced by aerosols that accumulate in the central Arctic, being located at the boundary and sometimes within the vortex. Flow to ALT also occurs directly from Siberia (Sharma et al., 2006) and over the North American high pressure ridge and possibly up through Baffin Bay associated with anti-cyclonic flow over Greenland.

BRW is impacted by aerosols that accumulate in the central Arctic in associated with flow around the Beaufort Anticyclone and by long-range transport from Asia when aerosols are carried out over the North Pacific Ocean and entrained along the boundary of the Aleutian Low. These dominate flow patterns are shown in Fig. 1(a) with shorter vectors indicating the arrival of the aerosol at the respective sites. Note; these represent mean patterns only during spring, which may vary during other seasons and from year to year. Year-to-year

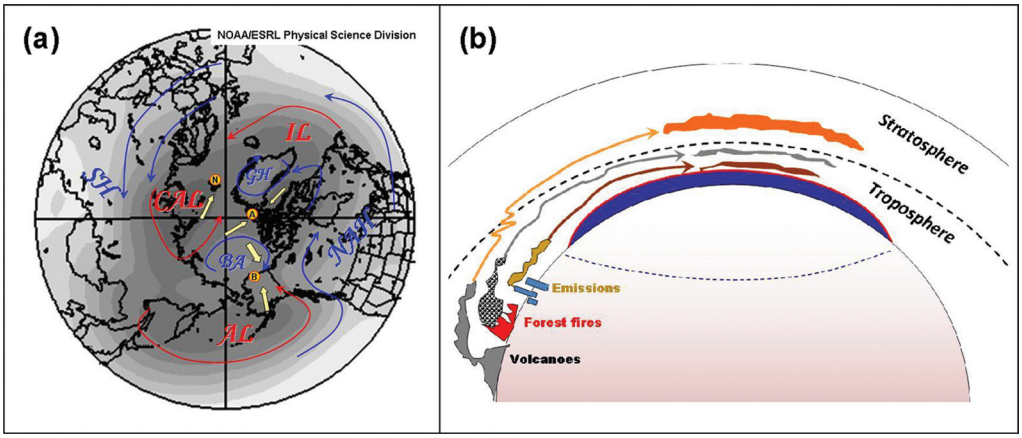

Figure 1

Long-range transport of aerosols into the Arctic.

(a) Mean 850 mb geopotential height field for March/April/May 2001–2011, with darker regions corresponding to low pressure centers. The primary high and low pressure centers are indicated; designated as follows: Siberian High (SH), Aleutian Low (AL), Beaufort Anticyclone (BA), North American High (NAH), Icelandic Low (IL), Central Arctic Low (CAL), and Greenland High (GH). Blue and red arrows indicate air flowing around the highs and lows, respectively, on the basis of the corresponding mean vector wind fields (not shown). Large yellow vectors indicate trajectory of arrival relative to BRW (B), ALT (A) and NYA (N), respectively. (b) Schematic, vertical cross-section of aerosol transport into the Arctic from lower-latitude source regions. Arrival height is dependent on the latitude and manner of release. The blue dome represents the persistent surface-based temperature inversion that inhibits mixing of aerosol to the surface.

doi: 10.12952/journal.elementa.000027.f001

variations are evident when comparing the transport of aerosol into the Arctic; e.g., April 2009 versus April 2008. During the 2009 PAMARCMiP (Polar Airborne Measurements and Arctic Regional Climate Model Simulation Project) airborne campaign, Stone et al. (2010; Fig. 1, Fig. 4(a)) observed relatively high aerosol loading above the aircraft when flying at altitudes < 160 m over regions of the Arctic Ocean, between Svalbard and Alaska. The aerosol was transported from Eurasia due to a coupling of an anticyclone centered over western Russia/Europe and a Low centered over the Kara Sea. During April 2008, in the Alaskan Arctic, Brock et al., (2011; references therein) observed abnormally early incursions of smoke from biomass burning (BB) in southern Russia and southeastern Siberia. The smoke plumes were observed above ~1600 m altitude (Brock et al., 2011; Fig. 3), while the boundary layer remained relatively clean. The contrast observed during successive years is a testament to the fact that Arctic aerosols are highly variable in time and space, making climate assessments challenging. Studies of source regions of BC at BRW (1991–1999) have shown that South and Eastern Siberia are the predominant areas of influence due to large-scale mining and industrial activities there (Polissar et al., 2001).

Fig. 1(b) is a schematic that illustrates the layering of aerosols in the Arctic as a function of where and how they are released into the atmosphere. A surface-based temperature inversion is a persistent feature of the Planetary Boundary Layer (PBL) during most of the year (e.g., Kahl, 1990). The inversion inhibits mixing of aerosol to the surface. As explained by Law and Stohl (2007), the dome of cold air forces air parcels to ascend along isentropic surfaces as they advect northward, arriving at altitude, leaving the PBL isolated. During winter, however, the polar dome can cover portions of Eurasia, where industrial pollutants are released continuously. Such emissions are transported at low levels and accumulate during winter and spring to produce a reservoir of "background haze" (Brock et al., 2011). Distinct from this background are aerosols that are episodically released into the atmosphere at lower latitudes. Desert dust and smoke from forest fires are lofted to high altitudes before being transported to the Arctic. Volcanic aerosols may infiltrate the Arctic stratosphere any time of year (e.g., Bourassa et al., 2010; O'Neill et al., 2012; Young et al., 2011), tend to have long residence times (Stone et al., 1993), and seldom mix to the surface (Law and Stohl, 2007). The layering of different aerosol types that varies throughout the season influences the AOD climatology of any particular site and further complicates evaluations of their radiative impact.

Sun photometry and the derivation of aerosol optical depth AOD

The derivation of spectral AOD from conventional Sun photometer observations made at BRW, ALT and NYA follow the practice of inverting the Bouguer-Lambert-Beer law to quantify the attenuation of direct solar radiation passing through the atmosphere. Instrumentation and processing procedures of data collected at BRW and ALT are described in Stone (2002) and for NYA by Herber et al. (2002). Similar devices used at the respective sites have been compared and cross-calibrated with other photometers used throughout the Polar-AOD network (Mazzola, et al., 2011). On the basis of these comparisons, the uncertainty of AOD measured (under clear skies) at the three stations is within ± 0.005 over the wavelength range, 500 nm to 862 nm (Mazzola, et al., 2011; Tables 2 and 3).

Here, we analyze spectral AOD at nominal central wavelengths of 412, 500, 675, and 862 nm (± 2 nm). Daily average values are computed from one-minute data and further averaged to monthly means to produce the climatologies. The one-minute data were screened to minimize the influence of thin clouds by evaluating temporal variations that generally differ between aerosols and clouds. The approach is used commonly to filter photometric data because clouds tend to be more tenuous and variable than aerosols (e.g., Smirnov et al., 2000). Cloud screening of photometric data is never perfect, however. Highly variable aerosol layers may be screened-out, while more homogenous layers of cloud pass through temporal filters. A second objective

test made on the basis of spectral signature of the aerosol/cloud has been found to be effective at high latitude sites. Thin cirrus is composed of large ice crystals that attenuate sunlight rather uniformly across the visible spectrum, whereas attenuation of light by aerosols tends to diminish with increasing wavelength. Details of cloud-screening procedures applied to the BRW and ALT data analyzed in this study are described in Stone et al. (2010). Variations within a running 11-minute data segment are first evaluated, screening values that exceed ± 0.015 as being contaminated, and then screened to filter data having spectral signatures observed commonly for thin cirrus clouds. As noted by Smirnov et al. (2000), spectral filtering is site-specific so this approach may not be appropriate at lower latitude sites. At NYA, coincident broadband irradiance data are used to determine if clouds are present by examining temporal variations subjectively, followed by an evaluation of spectral behavior to further distinguish aerosol from clouds. To our knowledge, uncertainties have not been assigned to any of these cloud-screening schemes owing to the site-specific nature of the problem. The inclusion of a few homogeneous cloud events is most likely offset by the exclusion of inhomogeneous aerosol events. Thus, climatologies generated from long time series of AOD are not prone to bias related to cloud screening as implemented here.

Results

Arctic aerosol optical depth (AOD) climatologies

Tomasi et al. (2012) characterize the optical properties of polar aerosols, presenting time series of AOD retrieved at a number of sites, including BRW for the period, 1977–2010, and NYA for the period, 1991–2010. They fitted each linearly to reveal any long-term trends. Slight increases in AOD at BRW and NYA were attributed to increased emissions and/or transport of pollutants to the Arctic from Eurasian industrial complexes over the past decade. Tomasi et al. (2014) updates these AOD climatologies and also includes results for ALT for 2004–2012. Following, we examine the time series (2001–2011) of AOD from BRW and NYA more closely and include an analysis of data collected at ALT for the period, 2004 through 2011.

We first present time series of daily mean spectral AOD and corresponding evaluations of Ångström exponent $\mathring{A}$ (or AE) for the wavelength pairs (λ_1, λ_2) that most closely match (412/675) and (500/862), where;

$$AE(\lambda_1,/\lambda_2) = -\log10(AOD(\lambda_1)/AOD(\lambda_2))/\log10(\lambda_1/\lambda_2) \quad (1)$$

AE is related inversely to mean particle size (Ångström, 1929; Ångström, 1964), and evaluations are commonly used to distinguish the relative fraction of fine and coarse mode particles in aerosol mixtures. The method of O'Neill et al. (2001a) exploits the naturally occurring curvature in spectral AOD to resolve the fraction of fine mode particles in the aerosol. Here, qualitative information about particle size and the relative fraction of fine versus coarse mode particles is obtained more simply by comparing values of AE(412/675) and AE(500/862) using equation (1), where central wavelengths can vary by ± 2 nm depending on the measuring device. For example, values of AE(412/675) ≤ 1.0 and ≥ 1.5 are indicative of relatively large and small particle dominance, respectively. Large dust particles tend to have small values, while small smoke particles have high values (Treffeisen et al., 2007; Fig. 7). Additional information is attained when comparing AE(500/862) with AE(412/675) because differences relate to spectral curvature that most aerosols display (O'Neill et al., 2001b). That is, the power-law relationship introduced by Junge (1955) is seldom realized in nature. For the purpose of this study, predominantly fine mode aerosols will display positive curvature, for which AE(412/675) < AE(500/862), and if there are a sufficient number of coarse mode particles in the mix, AE(412/675) > AE(500/862), as extrapolated from O'Neill et al. (2001b; Fig. 2). Thus, spectral signatures are valuable for distinguishing different types of Arctic aerosols.

Figure 2, *left panel pairs*, are time series of daily mean spectral AOD (*top;* color-coded by wavelength), and below each the corresponding records of AE(412/675) and AE(500/862) for BRW, ALT and NYA (*top to bottom*). Gaps occur over winter due to darkness, whenever data are missing due to operational problems, if deemed erroneous, and during periods of cloud cover. The y-axes are the same to facilitate comparisons. In each case, the time series of AOD at 500 nm is fitted linearly and also smoothed to help identify multi-year variations. The AOD(500) data are also fitted using a three-month smoother (black dots) to help reveal seasonal variations within each annual cycle.

Immediately below (*bottom, left* panel for each site) are the corresponding time series of AE(412/675) and AE(500/862) derived using eq. (1). Again, each series is fitted linearly and smoothed to highlight features particular to that location. The black dots represent the seasonally smoothed values of AE(412/675). Finally, the blue dots are the smoothed time series of the ratio, AE(500/862): AE(412/675) (*right scale*), that reveal variations in spectral curvature related to influence of fine versus coarse mode particles. A ratio of 1.0 would indicate the aerosol size distribution follows the Junge power-law relationship. Values of AE(500/862): AE(412/675) > 1.0 occur when spectral curvature is positive and there is a dominance of fine mode particles, such as for fresh smoke or volcanic aerosols. Negative curvature in the spectra occurs when a second, coarse

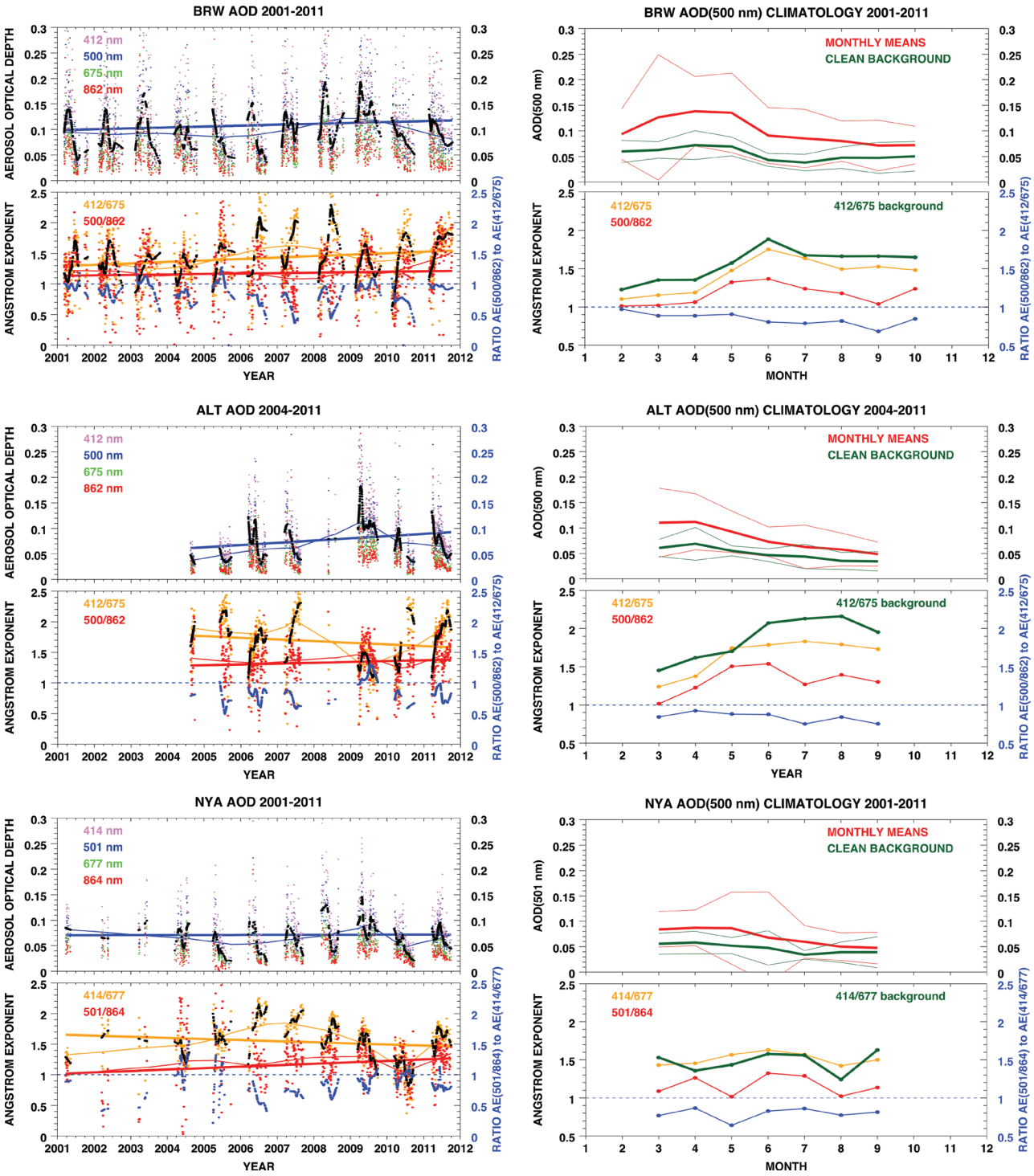

Figure 2

Stations daily time series and monthly climatologies of AOD.

AOD climatological data for (*top to bottom*) BRW, ALT and NYA (cross reference Table 1); (*left, upper panels*) are time series of mean daily spectral AOD at nominal wavelengths of 412, 500, 675 and 862 nn. AOD(500) (*blue*) has been fitted linearly and smoothed using a seven-year filter to indicate long-term variations. The AOD(500) series are also smoothed to show seasonal variations (*black*). (*left, lower panels*) are corresponding time series of AE(412/675) (*orange*) and AE(500/862) (*red*) (*left scale*), fitted and smoothed as for AOD. The seasonal variations of only AE(412/675) are highlighted in *black* and the seasonally smoothed ratio, AE(500/862): AE(412/675), in *blue (right scale*) to reveal changes in spectral signatures. (*right, top panels*) are monthly means (*bold*) ± 1σ (*thin*) values of AOD(500) derived from the corresponding daily values adjacent (red). In *green* are similar monthly evaluations for the clean background conditions as described in the text (*right, lower panels*) are monthly mean values of AE values according to color code and legends, with the *blue* curves giving the ratio referred to the *right scale*.

doi: 10.12952/journal.elementa.000027.f002

particle mode exists (e.g., O'Neill et al., 2001b; Fig. 2). On average, during the annual cycle, mean values of AE(500/862): AE(412/675) are < 1.0, indicative of bimodal particle size distributions. This does not mean, however, that particle number concentrations are dominated by large particles, only that a coarse mode exists. Episodically, an incursion of smoke and volcanic aerosol shows clear signatures of fine mode dominance (e.g., O'Neill et al., 2012; Saha et al., 2010). At BRW, in particular, there is a tendency for greater influence by coarse mode particles as summer progresses. This is attributed to an increase in the number of large sea salt aerosols present in the lower atmosphere as Arctic sea ice retreats each summer. Quinn et al. (2002; Fig. 2) document the increase in mass of super-micron size sea salts at BRW from winter through summer, resulting from wind-driven production and subsequent evaporation of sea spray. To a lesser degree, ALT shows a similar seasonal evolution, but not NYA, possibly due to factors related to flow patterns illustrated in Fig. 1.

Monthly AOD characterizations

The paired panels on the right side of Fig. 2 shows the climatologies in terms of monthly means derived from the adjacent daily time series. Only the AOD(500) climatology is plotted (*top panels, red curves*). Thin lines are the values at ± one standard deviation (1σ), used to gauge variability. We also define a monthly "background" (BG) value of AOD(500) (±1σ) (*green curves*). Background here is determined statistically by averaging all available minimum daily values for a particular month. For example, if the 2001–2011 time series were complete, we average 11 minimum daily values to produce that month's BG value. While the robustness of this approach diminishes for shorter time series, or in cases when data are missing, having site and month-specific BG values are useful when evaluating enhancements in AOD from the incursion of aerosols, whether pronounced or due to more subtle changes in atmospheric composition. Tomasi et al. (2012) used a different approach but with a similar objective, to evaluate small changes in AOD relative to clean background conditions. This topic will be elaborated upon in a following section. Note that background values have low standard deviations compared with the entire data set. This is due to the strict criteria applied in determining background values from only monthly minima. When all data are considered, AOD is highly variable in response to incursions of aerosols from lower latitudes, especially from late winter through spring.

Finally, monthly mean values of AE(412/675) and AE(500/862) are plotted in Fig. 2 (*right side, bottom panels*), along with AE(412/675) for background conditions only. The blue trace (*referenced to the right scale*) is the mean monthly ratio of AE(500/862) to AE(412/675), derived from corresponding daily values, adjacent. Table 1 summarizes the AOD and AE results numerically to facilitate comparisons.

Looking first at the monthly results (Fig. 2, *right side*), general characteristics of monthly mean AOD(500) and the clean BG at each site are revealed. We find that all sites display a springtime maximum in AOD and late summer minimum. On average, variability also decreases as the season progresses, with BRW being the most turbid and subject to the greatest variations throughout the cycle. NYA is the least perturbed site of the three, with ALT being slightly more turbid but having quite similar seasonal features. Differences relate to transport as was described above (Fig. 1(a)). BRW is influenced by northerly flow from Eurasia and by southerly flow from Asia. NYA is somewhat isolated in that flow form North America tends to pass to the south and flow from Eurasia involves a circuitous path across Siberia and around the Arctic vortex. At all three locations, seasonal background values show similarities with corresponding values of monthly total AOD; e.g., higher values during spring than summer, with NYA being the cleanest site. Background variability is similar at all locations.

In terms of spectral signatures (Fig. 2, *lower, right panels*), there is similarity in the annual cycle of AE(412/675) at all sites; low values in late winter, rising to a June/July maximum, and then decreasing late summer into autumn. The cycle is less pronounced at NYA, where more pristine conditions prevail throughout the year. The seasonal pattern suggests an increasing dominance of small particles as the Arctic vortex breaks up in spring, when hazy skies give way to more pristine conditions. Values of AE(500/862) are consistently lower than AE(412/675) at all locations throughout the seasonal cycle. Some divergence in values from spring through summer months at BRW and ALT result in small decreases in ratios of AE(500/862):AE(412/675). This is indicative of an evolving particle size distribution attributed to an increase in the number of large sea salt aerosols released into the atmosphere during late summer, when the Arctic sea ice is retreating (Quinn et al., 2002). We also find that values of AE(412/675) decline after June, a manifestation of a size distribution having an enhanced coarse mode.

Finally, the background aerosol also shows spectral evolution from winter through summer, mainly at BRW and ALT. Summer AOD minima correlate with peak values of AE(412/675), which occur when the aerosol is dominantly composed of small particles. During the most pristine periods, small particles suspended high in the troposphere and lower stratosphere probably make up the burden of aerosol because the low and mid troposphere is left relatively clean once the Arctic vortex breaks up in late spring. During the most pristine days, which are used to determine the 'clean background' climatology, larger sea salt aerosols are mainly absent.

Table 1. Monthly analyses of aerosol optical depth at 500 nm (nominal) and associated Ångström Exponents for channel pairs as noted in the footnotes; (cross reference Fig. 2).

BARROW 2001–2011									
Month	**AOD500**	**sd500**	**BG500**	**BGsd500**	**AE13**	**AE13bg**	**AE24**	**AEratio**	**days**
FEB	0.0937	0.0494	0.0598	0.0216	1.103	1.227	1.012	0.970	54
MAR	0.1264	0.1225	0.0626	0.0163	1.154	1.351	1.022	0.886	223
APR	0.1384	0.0679	0.0722	0.0285	1.188	1.353	1.063	0.885	198
MAY	0.1354	0.0778	0.0696	0.0183	1.475	1.572	1.323	0.905	133
JUN	0.0911	0.0546	0.0432	0.0126	1.750	1.882	1.365	0.805	195
JUL	0.0850	0.0568	0.0380	0.0161	1.634	1.673	1.237	0.787	181
AUG	0.0800	0.0392	0.0476	0.0211	1.493	1.661	1.177	0.817	65
SEP	0.0715	0.0494	0.0472	0.0302	1.526	1.662	1.039	0.682	43
OCT	0.0722	0.0368	0.0504	0.0290	1.481	1.647	1.236	0.845	46
ALERT 2004–2011									
MAR	0.1106	0.0678	0.0609	0.0165	1.240	1.452	1.016	0.843	62
APR	0.1122	0.0550	0.0690	0.0323	1.376	1.618	1.227	0.923	114
MAY	0.0927	0.0406	0.0551	0.0097	1.746	1.702	1.506	0.881	106
JUN	0.0731	0.0287	0.0468	0.0124	1.787	2.073	1.539	0.876	96
JUL	0.0630	0.0423	0.0439	0.0240	1.832	2.131	1.269	0.751	119
AUG	0.0577	0.0321	0.0354	0.0167	1.793	2.160	1.394	0.841	116
SEP	0.0487	0.0234	0.0347	0.0190	1.731	1.954	1.302	0.753	75
NY-ÅLESUND 2001–2011									
MAR	0.0843	0.0348	0.0559	0.0206	1.431	1.530	1.088	0.768	50
APR	0.0872	0.0352	0.0583	0.0222	1.455	1.357	1.264	0.867	98
MAY	0.0865	0.0710	0.0521	0.0157	1.566	1.435	1.017	0.641	110
JUN	0.0679	0.0899	0.0477	0.0336	1.630	1.578	1.325	0.828	112
JUL	0.0597	0.0320	0.0341	0.0083	1.569	1.560	1.289	0.861	102
AUG	0.0501	0.0271	0.0391	0.0198	1.422	1.242	1.023	0.774	61
SEP	0.0477	0.0311	0.0391	0.0304	1.500	1.629	1.137	0.814	40

AE13 is Ångström Exponent for the channel pair 1 and 3, nominally 412 nm and 675 nm AE(412/675)
AE24 is Ångström Exponent for the channel pair 2 and 4, nominally 500 nm and 862 nm AE(500/862)
AEratio is the ratio of AE(500/862) to AE(412/675)
BG represents the subset of background data on the basis of mean monthly minimum values of AOD(500)
sd is one standard deviation from mean values
days is the number of daily means used to perform the statistical analyses for respective climatologies

doi:10.12952/journal.elementa.000027.t001

Daily and long-term variations in AOD

Looking next at the daily time series of AOD(500) (Fig. 2, *left side, top panels*), we observe a long-term increase at BRW and ALT. We assign no statistical significance to this feature. The apparent trend is a result of abnormally high aerosol loading that occurred during 2008 and 2009, especially during spring. During spring 2008, incursions of smoke from biomass burning in Asia caused abnormally high aerosol loading in the Arctic (Warneke et al., 2009; Brock et al., 2011). The following spring, atmospheric circulation patterns were favorable for the transport of haze and dust into the central Arctic, again causing enhanced aerosol burdens over several weeks (Stone et al., 2010). The aerosols were widely dispersed and their signatures are obvious at all three monitoring sites. The minor volcanic eruptions at high latitude locations may have further enhanced AOD in the Arctic. As will be discussed in the following section, at times volcanic aerosols have been observed to increase AOD in the Arctic in recent years; evidenced by both satellite and ground-based systems (e.g., Stone et al., 2010; Young et al., 2011; O'Neill et al., 2012). Bourassa et al. (2012) gives an example of how the Asian Monsoon transport effluent from minor volcanoes into the stratosphere. The following section will discuss the potential impacts of minor volcanoes that occurred between 2006 and 2010. In subsequent years, the annual cycles of AOD and AE at all three locations return to climatological norms.

The spectral data show no coherent, long-term trend for the Arctic. AE values at BRW increased overall, while at ALT and NYA values of AE(412/675) have decreased and AE(500/862) have increased slightly. Significant data gaps at ALT and NYA make interpretation difficult. What is clear, however, is that spectral

signatures are ever changing in response to the transport of different aerosol types, seasonally and on multi-year time scales. The most common feature of all these time series is the maxima in AOD(500) in April, evidenced by the peaks in the smoothed data (black dots) each year. During April values of AE(412/675) tend to be low, while AE(500/862): AE(412/675) ratios are relatively large. The aerosol at this time of year is primarily made up of haze composed of moderate sized particles but may contain larger dust particles as well.

Analysis of background AOD time series

Tomasi et al. (2012) analyzed time series of summer BG AOD(500) for BRW and NYA and detected increases at both locations during the past decade. They suggest the increase at NYA is due to enhanced stratospheric loading resulting from minor volcanoes. Their analysis for BRW suggests possible additional contributions from Eurasian emissions and/or coal-burning in China. At tropical and mid latitudes, the stratospheric burden of aerosols has increased (Solomon et al., 2011). Their cooling effect may be contributing to a slow down in the rate of global warming in recent years. There is debate, however, regarding the source(s) of enhanced stratospheric aerosol. Hofmann, et al. (2009) suggested the observed increase in sulfate aerosol in the stratosphere since 2000 is due to increasing emissions from coal-burning in China. Through convection, the aerosol is lofted into the upper atmosphere and dispersed. Vernier et al. (2011) argue that the increase is due to "a series of moderate but increasingly intense volcanic eruptions" that have injected sulfur directly into the stratosphere. The recent study by Neely et al. (2013) gives further evidence that globally volcanic aerosols have increased the opacity of the stratosphere. In either case, once aerosols reach the stratosphere they can be transported to higher latitudes via the Brewer-Dobson circulation (e.g., Randel et al, 2006). To date, there has been little focus on the Arctic region with regard to the issue. Stone et al. (2010) noted an Arctic enhancement in upper atmosphere AOD during April 2009 only weeks after the eruptions of Mt. Redoubt in Alaska, giving evidence that plumes were drawn into the Arctic vortex during late March and early April that year. Young et al. (2011) simulated the regional radiative impacts of these plumes. O'Neill et al. (2012) documented an Arctic-wide dispersion of volcanic aerosols from the June 2009 Sarychev Peak eruptions. Subsequently, AOD increased regionally by as much as 0.05, an order of magnitude greater than normal for a quiescent stratosphere (Thomason et al., 2003; Yamanouchi et al., 2005).While it was once thought that minor volcanic eruptions had little and no lasting influence on high-latitude climate, the impact of more frequent and intense eruptions in recent years warrants investigation. The time series of BG AOD at Arctic sites can provide further insight.

The BRW, ALT and NYA background AOD time series were analyzed to determine if there is a coherent signal of an Arctic-wide enhancement in AOD in the past decade. Because background, as defined earlier, represents the most pristine conditions, any change is likely attributable to perturbations that occur in the upper atmosphere. A filtering process eliminates (most) influences from incursions of aerosols that impact the lower to middle atmosphere. The procedure is akin to that used by Solomon et al. (2011; Fig. 2) in their analysis of AOD minima data from the Mauna Loa Observatory (MLO) in Hawaii.

The monthly mean background AOD climatologies (Fig. 2, *right side, top panels*) are the basis for making an evaluation of upper atmospheric perturbations. Background values are site-specific and assigned by month, rather than setting a constant threshold as were done by Tomasi et al. (2012); they excluded values of AOD ≥ 0.08 from their analysis of only summer data. We prescribe monthly thresholds as being the mean background value, plus 1σ, derived from Fig. 2, listed in Table 1 as BG500 and BGsd500, respectively. A lower envelop of daily values is established as representing the cleanest days in the entire time series, while allowing +1σ of variation for the detection of small increases. All daily mean values of AOD(500) < (BG + 1σ) are plotted, fitted and smoothed as was done previously for the entire data set. The results are shown in Figure 3, by station (*top panels*) with analyses of their corresponding AE parameters immediately below. Note; for NYA, data prior to 2004 was excluded as being too sparse and poorly distributed. Given the disparity in the lengths of the time series and obvious data gaps, especially at ALT, a robust statistical analysis is not possible. Viewed collectively, however, there is a clear indication that the background aerosol has increased rather significantly over a vast region of the Arctic, with the greatest change occurring after 2005. The decadal increase in background AOD is on the order of 0.01, about double the AOD of an unperturbed stratosphere. Attribution is very difficult to assign without more observational evidence. We cannot rule out either of the two hypotheses put forth by others who documented similar increases at lower latitudes (e.g., Hofmann et al. 2009; Vernier et al. 2011). Most likely, both sources are involved. It is worth noting, however, that the most prominent rise occurs after a series of volcanic eruptions that began with the Soufriere Hills eruption in May 2006. Fig. 3 (*top panel*), indicates eruption dates of five eruptions that follow, named in the caption. The increase in background AOD at Arctic location is similar but weaker than that observed at MLO (Solomon et al., 2011; Fig. 2).

Spectrally (Fig. 3, *lower panels*), analyses of the background aerosol reveal similar features as shown in Fig. 2; *left, lower panels*, for the respective sites, although AE values are systematically greater than determined when all data are averaged (note; *scale change*). Again, these are difficult to interpret owing to short records and data gaps. A common feature is that the background aerosol is composed of smaller particles, on average,

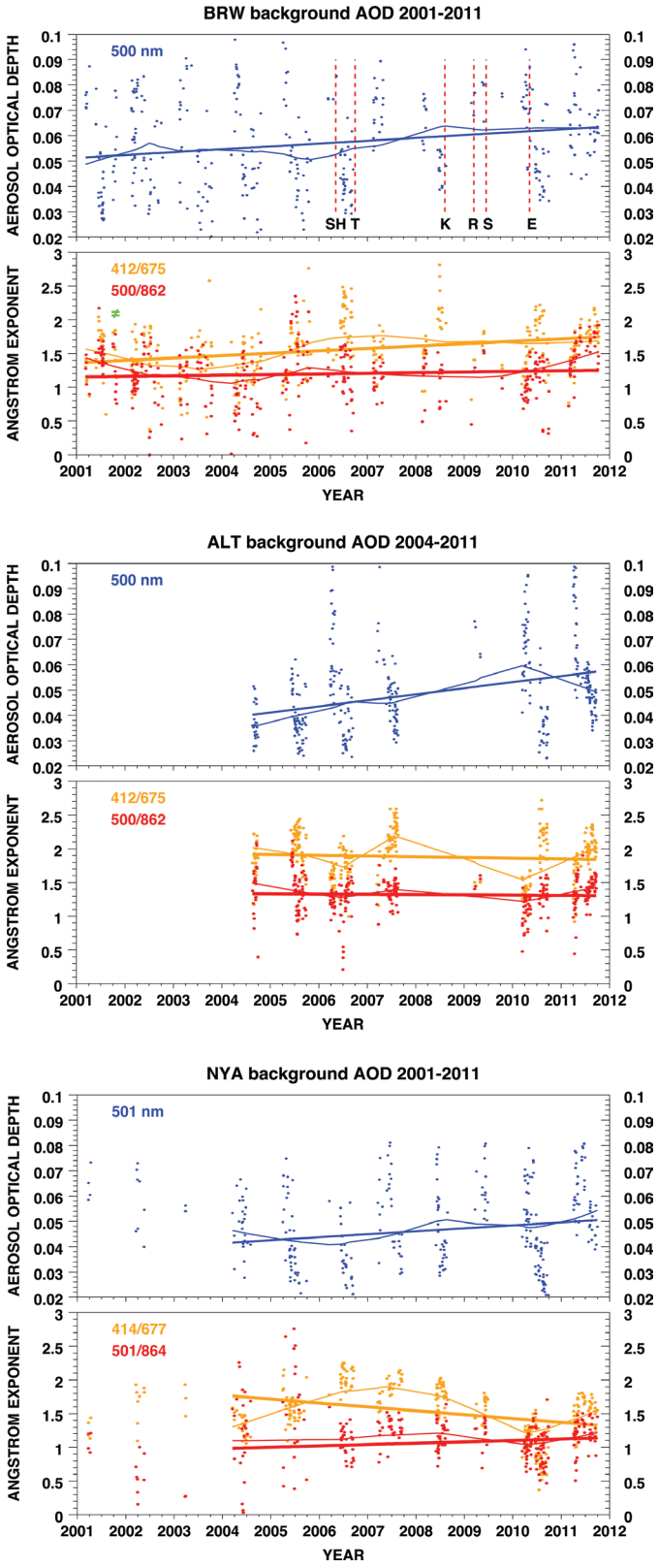

Figure 3

Daily time series of background AOD at stations.

(*top panels*) time series of daily mean AOD(500) for clean background conditions at BRW, ALT and NYA, fitted linearly and smoothed to show long-term variations. Six minor volcanic eruptions since 2005 are indicated, as follows: Soufrière Hills (May 2006) *Sh*, Kasatochi (August 2008) *K*, Tavurvur (October 2006) *T*, Redoubt (March 2009) *R*, Sarychev Peak (June 2009) *S* and Eyjafjallajokull (April 2010) *E*. (*lower panels*) corresponding derivations of AE for wavelength pairs as indicated in the legends used to evaluate spectral behavior of the background aerosol.

doi: 10.12952/journal.elementa.000027.f003

as evidenced by the larger values of AE. At BRW at least, the BG aerosol appears to have gotten smaller in recent years, possibly due to the production of very small sulfate particles in the stratosphere following minor volcanic eruptions, in combination with the transport of effluent from coal-burning in China as was suggested by Hofmann et al. (2009).

Analyses of black carbon concentrations in the Arctic

The measurement of the aerosol mass concentration of light absorbing carbon in the atmosphere, commonly referred as black carbon (BC), is especially important and has been the focus of many recent investigations pertaining to the changing Arctic climate. In the 1980s, the Arctic Gas and Aerosol Sampling Program (AGASP) (Schnell, 1984; Schnell et al., 1989) measured high concentrations of equivalent BC (EBC) in elevated layers north of Alaska. The results caused alarm because soot was known to absorb solar radiation, warm the atmosphere and accelerate snow and ice melt when deposited. The studies of Flanner (2013), Flanner et al. (2007) and Clarke and Noone (2007) have rekindled interest in BC, because the dramatic decline in Arctic sea ice (Stroeve et al., 2011) is partly attributed to the darkening effect of BC deposited on snow and ice (Hansen and Nazarenko, 2004; Flanner et al., 2007). Here, we investigate the records of EBC from BRW, ALT and NYA, derived using light absorption techniques. The data are compared with the AOD climatologies, and an assimilation of similar measurements made during Arctic air campaigns in order to better understand the vertical as well as horizontal distribution of BC in the Arctic since the 1980s.

Although the generic term, black carbon is used in this manuscript, separate terms such as EBC, rBC (refractory black carbon) and eBC (estimated black carbon) are also introduced in order to distinguish amongst different methodologies employed for the measurement of the BC mass concentrations in the snow as well as within the atmosphere. These are explicitly described in Table 1 of Appendix I. These definitions are consistent with those given by Petzold et al. (2013). In the following sections, light absorption-derived black carbon concentrations obtained by measurements made using Aethalometers (Hansen et al., 1982) or the Particle Soot Absorption Photometer (PSAP) will be referred to as EBC and vertical profiles of BC derived using the airborne, Single Particle Soot Photometer (SP2) will be referred to as rBC. The concentration of BC found in snow is referred to as eBC in accordance with the definition given by Doherty et al. (2010), or "the estimated true mass of black carbon per mass of snow." The determination of a measuring device's mass absorption coefficient (MAC) is necessary in order to convert light absorption to black carbon mass and applies to all optical filter-based techniques. The parameter is site specific because the composition and mixing of aerosol particles vary due to aging during transport and atmospheric composition and chemistry at the source. Instrumental specific features such as the filter material, humidity and airflow have an additional effect on these coefficients. Preliminary comparisons (unpublished) of BC mass concentrations measured using an SP2 and Aethalometer at Alert in 2011 revealed differences as large as a factor of 2 under certain conditions, especially during the Arctic haze period. Aethalometer measurements were also compared to thermal methods (Thermal Optical Transmittance) and EBC measurements agreed well with EC measurements at Alert and Ny-Ålesund during the winter/spring but a factor of two higher during summer at Alert (Sharma et al., 2002, 2004; Eleftheriadis et al., 2009). Aethalometers installed in aircraft used during spring campaigns during the 1980s were calibrated following the method of Gundel et al. (1984), with uncertainty estimated at ± 25% (Hansen and Novakov, 1989).

While there are uncertainties associated with each method, particularly the use of Aethalometers, by collecting continuous, long-term data and processing it consistently from site-to-site, time series can be evaluated for relative changes and are thus invaluable for climate assessments, as will be discussed below.

In situ measurements of equivalent black carbon; trends and climatologies

First we update and analyze in situ data collected at BRW and ALT since 1989 (Sharma et al., 2006), and the records from Zeppelin station (since 2001) (Eleftheriadis et al., 2009). Zeppelin station is adjacent to NYA, at an elevation of 464 m and is the most continuous record available in that region. The data were collected using Aethalometers at ALT and NYA and, at BRW, using an Aethalometer from 1989 to 1997 and a PSAP thereafter. A good description of their use and comparability is given by Sharma et al. (2002 and 2004). Both devices measure the attenuation of light transmitted through aerosols that accumulate on a filter. Despite intensive efforts, filter-based techniques have not yet determined a universal conversion of light attenuation signal to mass of black carbon (Baumgardner et al., 2012). The conversion of the light attenuation signal to light-absorbing carbon mass concentration is implemented by the choice of a mass-specific absorption coefficient (MAC) (Petzold et al., 2013). The resulting concentrations are reported as equivalent black carbon (EBC) as noted above. This coefficient can vary with time due to changes in the sources, atmospheric processing and mixing of light absorbing species with other aerosols, in addition to ambient operating conditions. To convert measurements of light absorption to EBC at the three observatories, site-specific values of MAC were determined for each type of instrument utilized. These are referred to specific attenuation coefficients (SAC). At ALT and BRW, the recommended values for SAC of 19 $m^2\ g^{-1}$ and 10 $m^2\ g^{-1}$ were

applied when using the Aethalometer and PSAP, respectively. A different model of Aethalometer in use at NYA has a SAC = 16.6 $m^2 g^{-1}$. Validations of Aethalometer EBC retrievals against results from thermo-optical analysis of elemental carbon mass have been made at Alert by Sharma et al. (2002 and 2004) and at Zeppelin station by Eleftheriadis et al. (2009). They found that by prescribing manufacturers' recommended attenuation coefficients at ALT, and by adjusting the coefficient at NYA to 15.9 $m^2 g^{-1}$, at least during winter/spring, derived values of EBC were comparable. Sharma et al. (2002) also demonstrated that EBC derived from an Aethalometer and PSAP are in fair agreement. This makes it possible to merge the two time series (1989–1997 and 1997–2011) at BRW. In general, however, accuracy of BC derived from the Aethalometer or PSAP is dependent on the assignment of site-specific attenuation factors, which vary seasonally with aerosol composition. Local dust during summer at ALT, for instance, reduces filter transmission, requiring larger attenuation coefficients be applied. Thus, the uncertainty in EBC measurements may be as large as 100% in some circumstances (Liousse et al., 1996; Sharma et al., 2002).

Figure 4 is a composite analysis of daily time series of EBC and respective monthly climatologies for the three sites. The left panels show all daily averages as gray traces and the winter (November through April) data as black dots. In each case, all data (gray), and the winter data only (blue), are fitted linearly and are also smoothed using a seven-year Lowess fraction (Chambers et al., 1983). The analysis updates that of Sharma et al. (2006), by adding data from 2004–2011, and includes the Zeppelin station (NYA) data. Note that we define winter to include all months in which EBC can accumulate in the snowpack and potentially lower the surface albedo at the time of snow melt. This snow darkening effect will be addressed in a following section.

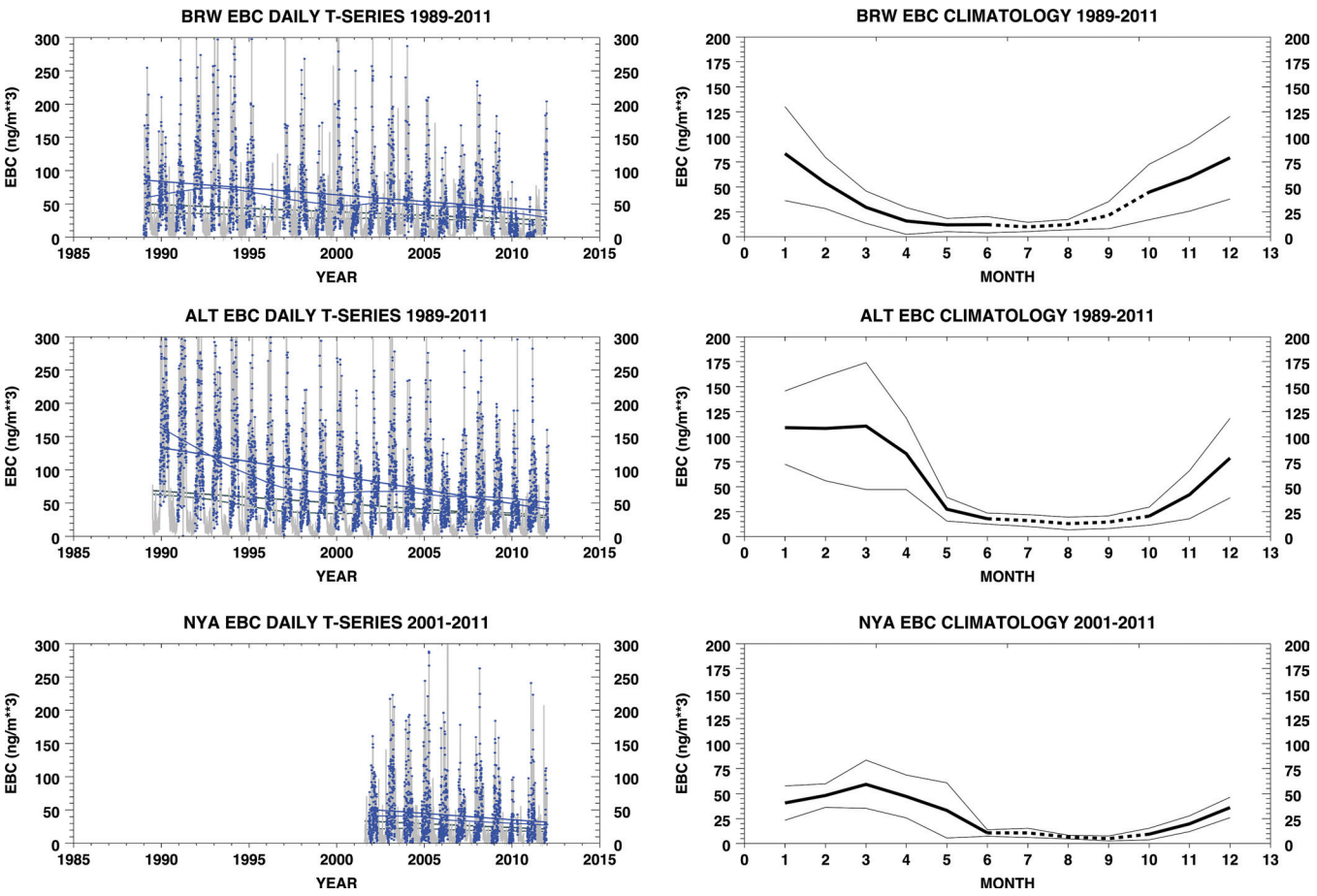

Figure 4

Station daily time series and monthly climatologies of EBC.

(*left panels*) time series of daily mean values of EBC (*gray*) at BRW, ALT and NYA. Winter data (*blue*) are fitted linearly and smoothed to show long-term variations. (*right panels*) respective monthly climatologies of EBC for the three sites. Monthly means are indicated by *thick* curves with ± 1σ indicated by *thin* lines. Dotted lines are periods with high uncertainty during summer months when absorption coefficients are variable.

doi: 10.12952/journal.elementa.000027.f004

EBC has decreased at all sites, although not linearly as evidenced by the smoothed curves. There are notable differences from site to site, in terms of magnitudes and variations over time. The findings are mostly consistent with those described in Sharma et al. (2006). Decreasing EBC in the Arctic is attributed to a combination of factors: 1) significantly diminished emissions from the former Soviet Union after 1990 and 2) changing atmospheric circulation patterns that influence the transport of carbonaceous aerosol from source regions (Hirdman et al., 2010; Sharma et al., 2013). A third factor is proposed by Garrett et al. (2011). They provide evidence that more efficient scavenging of aerosols during transport from lower latitudes results in cleaner air in the Arctic, irrespective of any change in transport. The process occurs through wet deposition, when atmospheric temperatures are near the freezing point and air is saturated. As a result of global warming, fewer aerosols (both scattering and absorbing types) may survive long-range transport to the Arctic, especially during the warm part of the year.

A pronounced decrease in EBC at ALT from 1989 to 1998 was followed by a slight increase through 2004; then a decline in the past several years. At BRW, EBC increased from 1989 until 1992, and then followed a similar trend as for ALT. And although the record for NYA does not begin until 2001 (missing the 1990s decline), a similar rise until 2004/2005 and subsequent decline is evident there as well. The most common feature is this slight rise and fall in EBC at the three sites over the past decade. This is notable because emission inventories have increased in the past decade (Ohara et al., 2007), owing in large part to increased coal-burning in China. The important point is that over a vast region of the Arctic, surface concentrations of EBC have decreased markedly since the late 1980s, with no apparent increase in the past decade in response to increasing emissions, particularly in China (Hofmann et al., 2009). During winter, EBC decreases from 1989 to present at ALT and BRW were about 70% and 50%, respectively, on the basis of the linear regressions shown in Fig. 4. The decadal (2001–2011) decrease at NYA was ≈ 37%. Corresponding decadal decreases at BRW and ALT from 2001 to present were about 37% and 21%, respectively (not shown). Note that we do not refer to these as trends, but rather as tendencies or overall changes. Statistical significance of any one-time series is questionable. Viewed as an ensemble, however, there is a climatically significant decrease indicated. The results reported above are in good agreement with those reported by Sharma et al. (2013) that show a 40% decline in EBC at BRW, ALT and NYA, overall, between 1990 and 2009. Further, the model they used resolves decreases in atmospheric BC regionally, showing a 50% decline over 16 years from sources in the Former Soviet Union. Another recent study by Stohl et al. (2013) shows the dramatic impact of emissions from gas flaring within the Arctic. Flaring is found to contribute about 50% of the simulated black carbon at the surface in during March in the Arctic. The observed decline in atmospheric BC is addressed in more detail in the following section.

The EBC climatologies for the three sites are presented in Fig. 4 (*right panels*). As for the AOD climatologies (Fig. 2), the mean ($\pm 1\sigma$) values for each month are plotted, derived from the daily data. Data from June through September (dashed) are prone to larger errors. As mentioned above, the accuracy of EBC derived from the Aethalometer or PSAP depends on the appropriateness of applied site-specific attenuation factors. These vary seasonally with aerosol composition. For instance, local dust contamination can reduce filter transmission that would require a larger attenuation coefficient be applied. In this study, values of SAC were applied in accordance with respective instruments uniformly over the year. Therefore, variations that relate to local contamination, particularly during summer, are not accounted for.

Late winter through summer cycles of EBC at ALT and NYA mimic their respective AOD climatologies for overlapping months, March through September (Fig. 2). Values of EBC and AOD peak during March typically. Both AOD and EBC decline thereafter to their summer minima. The correlation is not evident at BRW, however, where EBC concentrations peak mid winter and decline rather rapidly through spring, while AOD rises to an April/May maximum. The lack of correlation is understandable because the aerosols sampled near the surface do not generally represent the total column when a surface-based temperature inversion exists as it does most of the time during winter and spring at Arctic latitudes (e.g., Andrews et al., 2006). Transport, particular to BRW, is a likely factor. Less deposition at BRW during spring may result if more mixing with clouds and wet deposition occurs along the trajectory. Aerosols transported at higher altitudes, such as smoke from boreal wildfires and biomass burning, are less likely to be entrained along their path. Values of AE at BRW also increase by June (Fig. 2, *upper right*), indicative of small particle dominance possibly resulting from incursions of smoke from Siberia and North America. Although the smoke contains BC, it rarely mixes through the surface-based temperature inversion (Fig. 1(b)). The air aloft is effectively decoupled from the surface.

Unlike the extensive low-lying flat tundra site of BRW, where the inversion persists most of the time through spring, ALT and NYA are both elevated sites surrounded by complex terrain. Katabatic as well as synoptic, upper-level flow at these locations can mix the air more effectively, which may underlie the coupling of EBC and AOD at these sites (e.g., Beine et al., 2001).

A common feature at all sites is the increase in EBC by October, when fossil fuel consumption is on the rise in the northern hemisphere, sea ice and snow covers are being reestablished and the Arctic vortex takes form. Variations in EBC concentrations in the Arctic have been explained by variations in transport and deposition processes, including domestic sources (AMAP, 2011; Stohl et al., 2013). Finally, there are marked

differences in the magnitude of EBC at the three sites, ALT having the highest burden and NYA the lowest on an annual basis. As discussed above and at length by a number of investigators (e.g., Sharma et al., 2004; Quinn et al., 2007; Hirdman et al., 2010), atmospheric transport strongly influences the distribution of Arctic aerosols. High values of EBC at ALT are attributed, for instance, to efficient transport of effluents from Siberian sources across a frozen Arctic Ocean, whereas incursions reaching BRW often follow trajectories over the north Pacific, where particles can be scavenged through interactions with clouds and removed by wet deposition (Garrett et al., 2011). Thus, deposition of black carbon on Arctic snow is highly variable in space and time (Doherty et al., 2010), which in turn will affect its impact on climate.

Aircraft observations; vertical profiles of EBC and rBC concentrations

Aircraft measurements of BC have been derived using various instruments and methods. Historically, concentrations were derived from the filter-based absorption method using Aethalometers (Schnell, 1984; Schnell et al., 1989). As noted above, filter-based methods are prone to considerable uncertainty when converting light absorption to mass and the quantity measured is better referred to as equivalent black carbon (EBC). Therefore, EBC is only a proxy for the actual measure of BC mass. Aethalometers installed in aircraft were calibrated following the method of Gundel et al. (1984). At the time, measurement uncertainty was estimated to be ± 25% (Hansen and Novakov, 1989), but more recent evaluations show that errors of a factor of two can occur if incorrect site-specific absorption coefficients are prescribed during processing. In recent years, the use of the single-particle soot photometer, SP2, has gained favor but it too has relatively large uncertainty, ≈ 40% (Schwarz et al., 2006), depending on aerosol size distributions. It uses laser incandescence to detect individual soot particles in air and as particle size diminishes, retrievals are subject to greater uncertainty. When properly calibrated, however, accuracy to within about 15% is achievable (Laborde et al., 2012). The quantity retrieved is often referred to as refractory black carbon, or rBC.

Figure 5 is a chronology of atmospheric EBC and rBC ensemble profiles obtained during several Arctic aircraft campaigns. The legends denote which campaign, by month(s)/year, and the number of profiles in each ensemble average. For sake of clarity, only averaged or smoothed profiles are shown. Variations are significant, both spatially and temporally. In 1983 and 1986, Arctic Gas and Aerosol Sampling Program (AGASP) flights were flown over the Alaskan and Canadian Arctic as far East as Greenland (Schnell, 1984; Schnell et al., 1989). Using an Aethalometer on board the NOAA WP-3D, Hansen and Novakov (1989) measured concentrations of EBC in the range of 300–500 ng m^{-3} at low altitudes and 25–100 ng m^{-3} above 8 km. The profiles labeled AGASP-II and AGASP-I in Fig. 5 are derived from figures 7 and 8, respectively of their paper.

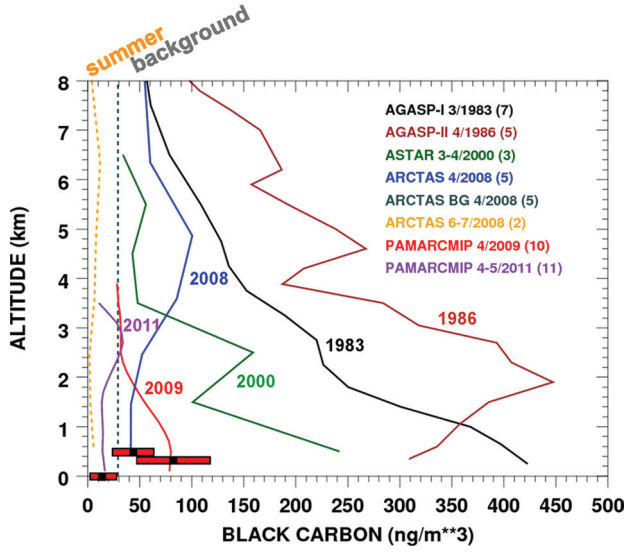

Figure 5

Profiles of black carbon concentrations from Arctic aircraft campaigns.

Ensemble average profiles of black carbon (EBC or rBC) concentration measured during Arctic aircraft campaigns, labelled chronologically (*from top*). Each represents a temporal and spatial average of the number of individual profiles indicated within parentheses, by month(s)/year. The gray dashed line represents the clean background value measured in the Alaskan Arctic during April 2008. Note, the yellow dashed line is for one summer, 2008. Climatological means (± 1σ) of EBC measured during April at BRW, ALT and NYA (*by elevation, respectively*) are indicated by black symbols and red bars, respectively (from Fig. 4). Further details and references are given in the text.

doi: 10.12952/journal.elementa.000027.f005

Only three profiles are averaged (from Aethalometer data) collected during the spring 2000 Arctic Study of Tropospheric Aerosol and Radiation (ASTAR) campaign conducted from Longyearbyen, Svalbard (Yamanouchi et al., 2005), one obtained during a haze event that occurred in the vicinity of Ny-Ålesund.

The spring and summer 2008 Arctic Research of the Composition of the Troposphere from Aircraft and Satellites (ARCTAS) campaigns were conducted mainly in the Alaskan Arctic and Greenland, respectively, with profiles of rBC derived from an SP2 on board the NASA DC-8 aircraft (Matsui et al., 2011). In this instance, median rather than mean profiles are plotted in Fig. 5 (provided by H. Matsui, personal communication).

Next, an ensemble average of 10 profiles, derived from an SP2 on board the Alfred Wegener Institute (AWI) BT-67 aircraft (Polar-5) during April 2009 is reproduced (Stone et al., 2010; Fig. 7(f)). These 10 profiles were collected during the first PAMARCMiP campaign (Herber et al., 2012; Hoffmann et al., 2011). Preliminary results from the spring 2011 PAMARCMiP campaign are also presented; an average of 11 profiles derived using a SP2 on board Polar-5. Of these, three were made near BRW in early April, seven in the vicinity of ALT, mid April, and one near NYA in early May.

As reference for evaluating the ensemble average data, the gray dashed line in Fig. 5 represents the April 2008 "background value" of atmospheric rBC, as defined by Warneke et al. (2010). Brock et al. (2011) refer to air masses of this type as "background haze" to distinguish the free tropospheric air from cleaner Arctic boundary layer (ABL) air, and from elevated incursions of pollutants or plumes of smoke from biomass burning.

What insight can we gain from Fig. 5? Unfortunately, there is no continuous time series of vertical atmospheric BC in the Arctic. There are relatively few profiles, spanning nearly thirty years, to evaluate. They are disparate in time and space and measurement strategies have changed over the years. Even the more direct measure of rBC using the SP2 is subject to large uncertainties (Appendix I). Still, there is an indication that atmospheric concentrations of BC (EBC and rBC) have decreased in recent decades. The early AGASP flights revealed large inter-annual variability in the vertical structure of EBC, but during no campaign since have such high (average) concentrations been measured, even if AGASP data are biased high by as much as a factor of two, the high range of uncertainty for the Aethalometer (Appendix I). It is notable that coincident AOD measurements made during AGASP-I were in the range 0.22 to > 0.4 (Bodhaine et al., 1984) and during AGASP-II up to 0.7 (Dutton et al., 1989). Such values exceed, by > 1σ, the 2001–2011 March/April BRW AOD climatology presented in Fig. 2. Abnormal burdens of EBC measured during the respective campaigns (Fig. 5) are consistent with these abnormally large AOD values and give credence to the validity of the original Aethalometer data from those early flights.

Year-to-year variations in atmospheric EBC continue to be observed, but perturbations appear moderate compared with measurements made during the 1980s. We emphasize here that the data presented in Fig. 5 represent snapshots, which give only a cursory view of the true temporal and spatial variations in the vertical distribution of BC (EBC & rBC) in the Arctic. There are no predictable annual cycles, as is evidenced by comparing rBC profiles from April 2008, 2009 and 2011. April 2008 and April 2009 were characterized as having high AOD during spring relative to the 2001–2011 climatologies (Fig. 2). During April 2008, in the Alaskan Arctic, relatively high concentrations of rBC were measured at mid levels of the atmosphere, attributed to direct transport of biomass smoke from southern Russia and southeast Siberia (Warneke et al., 2009). In contrast, during 2009 there were few aerosol layers observed aloft, but concentrations of rBC were relatively high near the surface, attributed to a rather persistent incursion of effluents from Eurasia (Stone et al., 2010). The ensemble-average of 11 profiles analyzed for spring 2011 reveal very clean conditions at low levels and moderate rBC loading at mid levels, noting that during six flights made in the vicinity of ALT, daily mean AOD (500) values were at background levels (< 0.07). During the spring 2004 ASTAR campaign, the AWI Dornier Do228 (Polar-2) aircraft was operated from Longyearbyen, Svalbard. The air was relatively pristine and EBC concentrations were below the threshold of the Aethalometer; the "air was too clean to measure absorption coefficient" during the normal flight segments made over several minutes (S. Yamagata, private communication).

Finally, corresponding climatological values of EBC, measured at the three ground sites during April, are plotted according to their respective elevations in Fig. 5, bars; *lower left*. For each station, the April mean concentration (± 1σ) is shown. The fact that recent (2008–2011) mean profiles of rBC, derived from aircraft measurements, are in good agreement with the station EBC climatologies suggests that the historic, ground-based Aethalometer- and PSAP-derived values of EBC are a reasonable proxy for black carbon in the Arctic, at least during spring. Although not shown in Fig. 5, the standard deviation of aircraft measurements of rBC tend to exceed those of EBC indicated by the red bars. Standard deviation of rBC profiles during the 2009 PAMARCMIP campaign were in the range ± 60 ng m^{-3} (Stone et al., 2010; Fig. 7f), versus ± 15–35 ng m^{-3} at similar elevations of the ground stations. The older aircraft profiles of EBC (from AGASP and ASTAR flights) fall well outside the range of ground-based observations, however. As noted above, few profiles were made during the early campaigns and some of those were made during anomalously turbid periods, and as such may not be entirely representative. EBC derived from Aethalometer or PSAP measurements are not directly comparable to measurements of rBC, and yet we find good agreement at the respective elevations of the ground stations in recent years.

Collectively, the evidence in Fig. 5 suggests that atmospheric black carbon concentrations in the Arctic atmosphere have decreased substantially since the 1980s, which is consistent with the downward trends of EBC measured at BRW, ALT and NYA (Fig. 4). This holds true even if the AGASP data are biased high. As mentioned earlier, coincident large values of AOD reported by Bodhaine et al. (1984) and Dutton et al. (1989) give credence to the AGASP observations, although we cannot be sure those data are generally representative of the Arctic during that period.

The differences between present-day concentrations of rBC and EBC from the 1980s likely result from changing emission inventories and atmospheric circulation patterns described in the previous section. The decrease in industrial emissions from the former Soviet Union during the early 1990s is probably a major factor. Decreases in atmospheric BC most likely underlie the trends in near-surface concentrations of EBC (Sharma et al., 2004 and 2006), noting that effluents must first be transported from distant source regions aloft before being deposited or mixed to the surface (Fig. 1).

Evaluation of estimated black carbon (eBC) concentrations in Arctic snow

Further evidence of diminishing BC in the Arctic comes from a recent survey of soot concentrations measured in the annual snowpack. Doherty et al. (2010) summarize results from surveys made 1998 and 2005–2009. They repeated measurements made in 1983–1984 (Clarke and Noone, 1985), extending coverage to eastern Russian and into the central Arctic. Although the recent (~ 1200) samples were processed differently than those (60) from the earlier survey, Doherty et al. (2010) conclude that estimates of BC concentrations in snow have decreased over the Arctic as a whole. Regional changes were found to be significant. By referring to Doherty et al. (2010; Table 9), comparisons of the historical snow surveys with our trends in EBC (Fig. 4) are possible. Results of the survey give estimates of black carbon concentration in snow, hereafter referred to as eBC to distinguish this measure from the in situ measure of equivalent BC, EBC, or direct measure of BC, rBC (Appendix I). Values of eBC are inferred using spectrophotometry. Snow samples are melted through filters and analyzed by comparing their transmittance with calibrated standard filters containing known amounts of Monarch-71 soot (Doherty et al., 2010). Their summary table compares median eBC concentrations in snow measured during the 1983/1984 and the more recent survey, by region. Cross-referenced with the map showing where snow samples were collected (Doherty et al., 2010; Fig. 2), we find reasonable co-location of three of their regions with BRW, ALT and NYA. The corresponding regions defined in Table 9 of Doherty et al. (2010) are Alaska, Canada (Arctic) and Svalbard, where relative percent decreases in eBC from 1983/1984 through 2009 were ~ 40%, 62% and 36%, respectively. By refitting the winter (November–April) time series shown in Fig. 4 only through 2009 the following changes in EBC are estimated: BRW (1989–2009), 45%, ALT (1990–2009), 68% and NYA (2001–2009) 37%. Although the time series of average winter EBC and samples of eBC concentrations in snow collected during spring are not matched in time, we find that long-term decreases are of similar magnitudes. Changes in snow eBC and EBC vary by location but also show consistency from region-to-region. Northern Canada (ALT) shows the most dramatic decline (snow eBC, 62%; EBC, 68%) and Svalbard (NYA) the least decline (snow eBC, 36%; EBC, 37%). There is a risk associated with making such comparisons because there are effectively only two data points from which to evaluate changes in eBC concentrations in snow, compared with continuous time series of EBC from the stations. For example, it is possible that eBC concentrations in Arctic snow increased after the 1983/1984 surveys were conducted before eventually declining, but we have no data to determine the year-to-year variations. Also, sites where snow and air samples are collected are not generally co-located, so direct comparisons are not possible. If we do assume the snow surveys made in Alaska, the Canadian Arctic and in Svalbard are representative of our respective ground stations within those regions, however, then the 20^{+} year decreases in eBC in snow (Table 9 of Doherty et al., 2010) are quite consistent with the long-term decreases in EBC measured at BRW, ALT and NYA (Fig. 4) and also the chronology of EBC and rBC aircraft profiles (Fig. 5). An overall, downward trend in BC in the atmosphere (near and at the surface) since the 1980s is observed.

Summary of results

There has been a resurgence of interest in Arctic aerosols in recent years, motivated by the dramatic decline in Arctic sea ice since 1979. Black carbon (soot) has been identified as a warming agent. Nordenskiöld (1883) first called attention to the potential impacts of BC over a century ago, but few measurements of aerosol properties were made in the Arctic before the 1970s. Decades after establishing baseline observatories in the Arctic, conducting a number of aircraft campaigns and the deployment of polar orbiting satellites, the role of Arctic aerosols is still not well understood. The network of ground stations is sparse, air campaigns are few and far between, and remote sensing data are still prone to large uncertainties. As a consequence, a reliance on regional and global climate models has evolved for assessing climate impacts of aerosols (e.g., Bond et al., 2013; Flanner et al., 2007; Shindell and Faluvegi, 2009; Sand et al., 2013). Climate models provide valuable insights about processes and impacts and thus are the basis for making impact assessments and establishing policy. GCM results, however, are also prone to large uncertainties.

Rapid warming at high northern latitudes is partly attributed to long-range transport of BC from various sources, in large part due to the incomplete combustion of fossil fuel (AMAP, 2011; references therein). BC absorbs sunlight, warming the atmosphere and surface when deposited on snow and ice. The darkening effect accelerates the annual melt and induces a temperature-albedo feedback. Cause and effect have not been well-established empirically, however, because small decreases in albedo due to soot deposition are very

difficult to distinguish from much larger variations that occur naturally. Measuring eBC deposition on snow and ice on temporal and spatial scales with sufficient accuracy to quantify its effect is not feasible at present.

The temporal and spatial distributions of aerosols in the Arctic atmosphere are also highly variable owing to changing emission inventories and circulation patterns that determine transport from source regions. Airborne campaigns have provided valuable snapshots in time and space from which to characterize the aerosol and assess climate impacts when combined with surface-based observations. The assimilation of multiple data sets can be used to verify climate model simulations and validate satellite retrievals of surface and atmospheric properties.

This study emphasizes the value of long-term observations and performing empirical analyses to characterize Arctic aerosols. To provide context, transport processes are described and primary pathways to three baseline observatories, BRW, ALT and NYA, are identified (Fig. 1). The widely distributed sites are shown to represent distinct regions in terms of aerosol climatologies. Station climatologies of AOD (Fig. 2) and EBC (Fig. 4) are presented; their similarities and differences discussed, including long-term variations in daily time series. An analysis of clean background conditions is also made (Fig. 3).

A collection of aircraft profiles of EBC and rBC, spanning nearly three decades, are assimilated and compared (Fig. 5) to determine if there have been changes that correlate with ground observations.

The combined analyses provide broad context for understanding and evaluating key properties of Arctic aerosols and their climate impacts, both historically and for purposes of establishing a baseline for future impact assessments, and in particular pertaining to black carbon. Findings are summarized below:

- Northern hemisphere atmospheric circulation patterns (Fig. 1) determine pathways for the transport of aerosols into the Arctic, which underlie spatial variations in AOD (Fig. 2) and EBC (Fig. 4); e.g., the western Arctic (BRW) is more turbid than the European Arctic (NYA)
- Seasonal cycles of AOD are pronounced and vary spatially owing to changing emissions, aerosol composition and circulation patterns that affect transport and deposition rates along pathways; pollution haze and dust are most common in spring, while biomass and wildfire smoke are observed from late spring through autumn
- AOD spectral signatures derived from Ångström exponents vary on seasonal to decadal time scales and are indicative of changing particle size distributions (Fig. 2 and Fig. 3)
- Vertical distributions of Arctic aerosols are highly variable, depending to some extent on latitude where emitted (Fig. 1); e.g., Eurasian haze tends to accumulate at low levels and smoke in elevated layers; mixing is inhibited most of the year by a persistent surface-based temperature inversion
- An analysis of background AOD(500) for 2001–2011 shows an increase in the Arctic, presumably at high altitudes, attributed to an accumulation of sulfate particles from coal-burning in China and increased volcanic activity
- An Arctic-wide decrease in EBC is evidenced near the surface (Fig. 4) and in the atmosphere (Fig. 5), attributed to decreased emissions and most pronounced after the break-up of the Soviet Union
- Due to decreases in EBC since the 1980s, present-day deposition of black carbon is expected to be lower than during past decades; thus the darkening effect of BC in snow is not likely a major contributor to recent declines in Arctic sea ice melt

Discussion and concluding remarks

The findings of this study are specific to the Arctic region. Studies, e.g., Shindell and Faluvegi (2009), Shindell et al. (2010) and Sand et al. (2013), address the sensitivity of Arctic climate to mid-latitude warming, attributed in part to solar absorption by black carbon emitted from industrial areas. With regard to deposition of BC in the Arctic, Bond et al. (2013) state: "The best estimate of climate forcing from black carbon deposition on snow and sea ice in the industrial era (1750–2005) is +0.13 W m^{-2} with 90% uncertainty bounds of + 0.04 to + 0.33 W m^{-2}." Sand et al. (2013) provide a simulated assessment of mid-latitude versus in-Arctic impacts of atmospheric BC. Their calculations "show that increased BC forcing in the Arctic atmosphere reduces the surface air temperature in the Arctic with a corresponding increase in the sea-ice fraction…." Further, they state that: "The analysis indicates that this effect is due to a combination of a weakening of the northward heat transport caused by a reduction in the meridional temperature gradient and a dimming at the surface."

The degree of warming by BC at mid-latitudes is currently in question. When soot particles are mixed internally with other aerosols, absorption is enhanced due to a lens effect of the liquid, spherical shell around the absorbing particle (e.g., Chylek et al., 1995). Impacts will vary in proportion to the absorption enhancement (E_{abs}) that occurs in the vicinity of the source, which is not well known. Estimates of E_{abs} vary widely, depending on whether theoretical or empirical methods are employed. Cappa et al. (2012) measured values of $E_{abs} \approx 0.06$ in the vicinity of urban areas of California, whereas theoretical and laboratory estimates range from 2 to 2.5. It is beyond the scope of this study to evaluate the potential impact of mid-latitude warming by BC on Arctic climate. Cappa et al. (2012), however, conclude that models are potentially overestimating E_{abs} by as much as a factor of 2 and therefore the benefits of BC mitigation globally would be similarly overestimated.

Efforts to quantify the darkening effect of BC deposited in the Arctic empirically should be a priority so that direct comparisons with dimming effects are possible. If the effect is measurable, then careful monitoring of eBC concentrations in snow over the annual cycle, in combination with spectral albedo measurements, may resolve a signal. More automated sampling of snow and aerosols during deposition must also be developed. The measurements will need to be made in conjunction with other radiometric observations now being made at Arctic observatories.

It is clear that forcing varies significantly, both temporally and spatially, as the melt season progresses, depending on aerosol composition and loading, day length and surface albedo. A good illustration of this is can be found in Sand et al. (2013). Their Figure 13 shows a simulated annual cycle of net shortwave (SW) radiation at the surface, assuming BC concentrations in the Arctic for the year 2000. The combined impact of attenuation by atmospheric BC, changing albedo and sky cover results in approximately a 10 Wm^{-2} decrease from late winter to mid summer. Empirically, Stone et al. (2007; Table 1) and Stone et al. (2008; Table 1) quantify the direct SW radiative forcing caused, respectively, by Asia dust and wildfire smoke observed at BRW. Stone et al. (2008; Table 1), for example, measured the radiative forcing efficiency of smoke (defined as DARF in the study) to be less than –100 Wm^{-2} per unit of AOD at 500 nm when solar zenith angles are < 60° and the surface is free of snow. That is, for a modest loading of smoke having AOD(500) = 0.10, there results a net SW forcing of ≈ -10 Wm^{-2}, which radiatively cools the surface. Although such incursions are episodic, the cumulative dimming impact of atmospheric aerosols (BC + co-emitted species) over the annual cycle very likely more than offsets the darkening effects by BC estimated by Bond et al. (2013).

While today's chemical transport models, coupled with general circulation models are very sophisticated, further improvements are needed to account for sub-grid scale processes. Observational studies are also limited in scope and may not be representative of regional impacts, but offer valuable insights into processes that underlie regional climate response to aerosol forcing. The characterizations introduced here should be useful to constrain climate model simulations in the future. Further, empirical measurements of the darkening and dimming effects of Arctic aerosols are essential to validate climate models and improve assessments of aerosol impacts on Arctic climate. Also, when making impact assessments for the Arctic, the decadal trends in EBC (Fig. 4) cannot be ignored. If Arctic warming and sea ice decline are intrinsically linked to the transport and deposition of BC in the Arctic, then their long-term trends should be anti-correlated; they are not. Gauging from the tendencies in EBC shown in Fig. 4, Arctic-wide concentrations of EBC have decreased by ≈ 50% since the late 1980s, in large part due to diminished emissions from industrial complexes in northern Eurasia, particularly those in the Russian sector following the break-up of the Soviet Union. On the basis of two snow surveys (1983/1984 and 1998, 2005–2009), decreases in eBC concentrations in snow are consistent with our analyses of EBC at BRW, ALT and NYA. Current-day, surface EBC and atmospheric rBC concentrations are at modest levels. In effect, mitigation of BC relative to the Arctic has occurred already, although there has been no measureable solar brightening as may have been the case in Europe after the demise of the Former Soviet Union (Norris and Wild, 2007). Measures to further reduce the concentration of BC transported to the Arctic may not achieve the desired benefits. Polluted air in the Arctic is mostly composed of sulfates and organic carbon (e.g., Brock et al., 2011; Fig. 7) that scatter light efficiently. Any reduction in radiative forcing resulting from the mitigation of BC in the Arctic is likely to be more than offset by a warming (less cooling) effect as co-emitted aerosols are proportionally reduced. Further, mitigation is limited to anthropogenic pollutants (BC + co-emitted species) that have been in decline for decades (Fig. 4), while natural sources such as volcanic effluents, smoke from boreal forest fires and desert dust cannot be mitigated.

References

AMAP. 2011. The Impact of Black Carbon on Arctic Climate. AMAP Technical Report No. 4 (2011). Oslo, Norway: Arctic Monitoring and Assessment Programme (AMAP): 72 pp.

Andrews E, Sheridan PJ, Fiebig M, McComiskey A, Ogren JA, et al. 2006. Comparison of methods for deriving aerosol asymmetry parameter. *J. Geophys. Res* **111**: D05S04. doi:10.1029/2004JD005734

Ångström A. 1964. The parameters of atmospheric turbidity. *Tellus* **16**: 64–75.

Ångström A. 1929. On the atmospheric transmission of Sun radiation and on dust in the air. *Geogr. Ann* **11**: 156–166.

Baumgardner D, Popovicheva O, Allan J, Bernardoni V, Cao J, et al. 2012. Soot Reference Materials for instrument calibration and intercomparisons: A workshop summary with recommendations. *Atmos. Meas. Tech. Discuss* **5**: 2315–2362.

Beine HJ, Argentini S, Maurizi A, Mastrantonio G, Viola A. 2001. The local wind field at Ny-Ålesund and the Zeppelin mountain at Svalbard, Meteorol. *Atmos. Phys* **78**: 107–113.

Blanchet J-P. 1989. Toward estimation of climatic effects due to Arctic aerosols. *Atmos. Env* **23**: 2609–2625.

Bodhaine BA, Dutton ED, DeLuisi JJ. 1984. Surface aerosol measurements at Barrow during AGASP. *Geophys. Res. Lett* **11**(5): 377–380.

Bond TC, Doherty SJ, Fahey DW, Forster PM, Berntsen T, et al. 2013. Bounding the role of black carbon in the climate system: A scientific assessment. *J. Geophys. Res* **118**(11): 5380–5552.

Bourassa AE, Degenstein DA, Elash BJ, Llewellyn EJ. 2010. Evolution of the stratospheric aerosol enhancement following the eruptions of Okmok and Kasatochi: Odin-OSIRIS measurements. *J. Geophys. Res* **115**: D00L03. doi:10.1029/2009JD013274

Bourassa AE, Robock A, Randel WJ, Deshler T, Rieger LA, et al. 2012. Large volcanic aerosol load in the stratosphere linked to asian monsoon transport. *Science* **337**: 78. doi:10.1126/science.1219371

Brandt RE, Warren SG, Clarke AD. 2011. A controlled snowmaking experiment testing the relation between black carbon content and reduction of snow albedo. *J. Geophys. Res* **116**: D08109. doi:10.1029/2010JD015330

Brock CA, Cozic J, Bahreini R, Froyd KD, Middlebrook AM et al. 2011. Characteristics, sources, and transport of aerosols measured in spring 2008 during the aerosol, radiation, and cloud processes affecting Arctic Climate (ARCPAC) Project. *Atmos. Chem. Phys* **11**: 2423–2453. doi:10.5194/acp-11-2423-2011

Cappa CD, Onasch TB, Massoli P, Worsnop DR, Bates TS et al. 2012. Radiative absorption enhancements due to the mixing state of atmospheric black carbon. *Science* **337**: 6098. doi:10.1126/science.1223447

Chambers JM, Cleveland WS, Kleiner B, Tukey PA. 1983. *Graphical Methods for Data Analysis*. Duxbury Press. (Wadsworth & Brooks/Cole Statistics/Probability Series).

Chýlek P, Videen G, Ngo D, Pinnick RG, Klett JD. 1995. Effect of black carbon on the optical properties and climate forcing of sulfate aerosols. *J. Geophys. Res* **100**(D8): 16,325–16,332. doi:10.1029/95JD01465

Clarke AD, Noone KJ. 2007. Soot in the arctic snowpack: a cause for perturbations in radiative transfer. *Atmos. Environ* **41**(1): 64–72.

Doherty SJ, Warren SG, Grenfell TC, Clarke AD, Brandt RE. 2010. Light Absorption from Impurities in Arctic Snow. *Atmos. Chem. Phys* **10**: 1647–11680.

Dutton EG, Deluisi JJ, Herbert G. 1989. Shortwave aerosol optical depth of Arctic haze measured on board the NOAA WP-3D during AGASP-II, April 1986. *J. Atmos. Chem* **9**: 71–79.

Eleftheriadis K, Vratolis S, Nyeki S. 2009. Aerosol black carbon in the European Arctic: Measurements at Zeppelin station, Ny-Ålesund, Svalbard from 1998–2007. *Geophys. Res. Lett* **36**: L02809. doi:10.1029/2008GL035741

Flanner MG, Zender CS, Randerson JT, Rasch PJ. 2007. Present-day climate forcing and response from black carbon in snow. *J. Geophys. Res* **112**: D11202. doi:10.1029/2006JD008003

Flanner MG. 2013. Arctic climate sensitivity to local black carbon. *J. Geophys. Res. Atmos* **118**: 1840–1851. doi:10.1002/jgrd.50176

Fu PQ, Kawamura K, Chen J, Charrière B, Sempéré R. 2013. Organic molecular composition of marine aerosols over the Arctic Ocean in summer: contributions of primary emission and secondary aerosol formation. *Biogeosciences* **10**: 653–667. doi:10.5194/bg-10-653-2013

Fuller KA, Malm WC, Kreidenweis SM. 1999. Effects of Mixing on Extinction by Carbonaceous Particles. *J. Geophys. Res* **104**: 15941–15954.

Garrett TJ, Brattström S, Sharma S, Worthy DEJ, Novelli P. 2011. The role of scavenging in the seasonal transport of black carbon and sulfate to the Arctic. *Geophys. Res. Lett* **38**: L16805. doi:10.1029/2011GL048221

Grenfell TC, Light B, Sturm M. 2002. Spatial distribution and radiative effects of soot in the snow and sea ice during the SHEBA experiment. *J. Geophys. Res* **107**: 8032. doi:10.1029/2000JC000414

Gundel LA, Dod RL, Rosen H, Novakov T. 1984. The relationship between optical attenuation and black carbon concentration for ambient and source particles. *Sci. Total Environ* **36**: 197–202.

Hansen ADA, Rosen H, Novakov T. 1982. Real-time measurement of the absorption coefficient of aerosol particles *Appl. Opt* **21**: 3060–3062.

Hansen ADA, Novakov T. 1989. Aerosol black carbon measurements in the Arctic haze during AGASP-II. *J. Atmos. Chem* **9**: 347–361.

Hansen J., Nazarenko L. 2004. Soot climate forcing via snow and ice albedos. *Proc. Natl. Acad. Sci* **101**(2): 423–428.

Hadley OL, Kirchstetter TW. 2012. Black-Carbon reduction of snow albedo. *Nature Climate Change* **2**: 437–440. doi:10.1038/Nclimate1433

Herber A, Thomason LW, Gernandt H, Leiterer U, Nagel D, et al. 2002. Continuous day and night aerosol optical depth observations in the Arctic between 1991 and 1999. *J. Geophys. Res* **107**(D10): 4097. doi:10.1029/2001JD000536

Herber AB, Haas C, Stone RS, Bottenheim JW, Liu P, et al. 2012. Regular airborne surveys of Arctic sea ice and atmosphere. *Eos Trans. AGU* **93**(4): 41. doi:10.1029/2012EO040001

Hirdman D, Sodemann H, Eckhardt S, Burkhart JF, Jefferson A, et al. 2010. Source identification of short-lived air pollutants in the Arctic using statistical analysis of measurement data and particle dispersion model output. *Atmos. Chem. Phys* **10**: 669–693.

Hoffmann A, Osterloh L, Stone R, Lampert A, Ritter C, et al. 2011. Remote sensing and in-situ measurements of tropospheric aerosol, a PAMARCMiP case study. *Atmospheric Environment* **52**: 56–66. doi: 10.1016/j.atmosenv.2011.11.027

Hofmann D, Barnes J, O'Neill M, Trudeau M, Neely R. 2009. Increase in background stratospheric aerosol observed with lidar at Mauna Loa Observatory and Boulder, Colorado. *Geophys. Res. Lett* **36**: L15808. doi:10.1029/2009GL039008

IPCC. 2007. *Climate Change 2007: The Physical Science Basis. Summary for Policy Makers. Contribution of Working Group I to the Fourth Assessment Report of the Intergovernmental Panel on Climate Change*. Cambridge, UK and New York, NY: Cambridge University Press: 996 pp.

Junge CE. 1955. The size distribution and aging of natural aerosols as determined from electrical and optical measurements in the atmosphere. *J. Meteorol* **12**: 13–25.

Kahl JD. 1990. Characteristics of the low-level temperature inversion along the Alaskan Arctic coast. *Int. J. Climatology* **10**: 537–548.

Kaufman YJ, Fraser RS. 1997. The Effect of Smoke Particles on Clouds and Climate Forcing. *Science* **277**: 1636. doi:10.1126/science.277.5332.1636

Laborde M, Schnaiter M, Linke C, Saathoff H, Naumann K.-H, et al. 2012. Particle Soot Photometer intercomparison at the AIDA chamber. *Atmos. Meas. Tech. Discuss* **5**: 3519–3573. doi:10.5194/amtd-5-3519-2012

Law KS, Stohl A. 2007. Arctic Air Pollution: Origins and Impacts. *Science* **16** (vol. 315, no. 5818): 1537–1540. doi:10.1126/science.1137695

Lindeman JD, Boybeyi Z, Gultepe I. 2011. An examination of the aerosol semi-direct effect for a polluted case of the ISDAC field campaign. *J. Geophys. Res* **116**: D00T10. doi:10.1029/2011JD015649

Liousse C, Cachier H, Jennings SG. 1993. Optical and thermal measurements of black carbon aerosol content in different environments: Variation of specific attenuation cross-section, sigma (s), *Atmos. Environ* **27**: 1203–1211.

Marks AA, King MD. 2013. The effects of additional black carbon on the albedo of Arctic sea ice: variation with sea ice type and snow cover. *The Cryosphere* **7**: 1193–1204. doi:10.5194/tc-7-1193-2013

Matsui H., Kondo Y, Moteki N, Takegawa N, Sahu LK, et al. 2011. Seasonal variation of the transport of black carbon aerosol from the Asian continent to the Arctic during the ARCTAS aircraft campaign. *J. Geophys. Res* **116**: D05202. doi:10.1029/2010JD015067

Mazzola M, Stone RS, Herber A, Tomasi C, Lupi A, et al. 2011. Evaluation of sun photometer capabilities for retrievals of aerosol optical depth at high latitudes: The POLAR-AOD intercomparison campaigns. *Atmos. Environ* **30**: 1–14. doi:10.1016/j.atmosenv.2011.07.042

Mitchell JM. 1957. Visual range in the polar regions with particular reference to the Alaskan Arctic. *J. Atmos. Terr. Phys* **17**: 195–211.

Neely RR III, Toon OB, Solomon S, Vernier J-P, Alvarez C, et al. 2013. Recent anthropogenic increases in SO_2 from Asia have minimal impact on stratospheric aerosol. *Geophys. Res. Lett* **40**: 999–1004. doi:10.1002/grl.50263

Nordenskiöld AE. 1883. Nordenskiöld on the inland ice of Greenland. *Science* **2**(44): 732–738. doi:10.1126/science.ns-2.44.732

Norris JR, Wild M. 2007. Trends in aerosol radiative effects over Europe inferred from observed cloud cover, solar "dimming", and solar "brightening." *J. Geophys. Res* **112**: D08214, doi:10.1029/2006JD007794

Ohara T, Akimoto H, Kurokawa J, Horii N, Yamaji K, et al. 2007. An Asian emission inventory of anthropogenic emission sources for the period 1980–2020. *Atmos. Chem. Phys* **7**: 4419–4444. doi:10.5194/acp-7-4419-2007

O'Neill NT, Dubovik O, Eck TF. 2001a. Modified Ångström Exponent for the Characterization of Submicrometer Aerosols. *Appl. Opt* **40**: 2368–2375.

O'Neill NT, Eck TF, Holben BN, Smirnov A, Dubovik O, et al. 2001b. Bimodal size distribution influences on the variation of Ångström derivatives in spectral and optical depth space. *J. Geophys. Res* **106**: 9787–9806. doi:10.1029/2000JD900245

O'Neill NT, Perro C, Saha A, Lesins G, Duck TJ, et al. 2012. Properties of Sarychev sulphate aerosols over the Arctic. *J. Geophys. Res* **117**: D04203. doi:10.1029/2011JD016838

Petzold A, Ogren JA, Fiebig M, Laj P, Li S-M, et al. 2013. Recommendations for the interpretation of "black carbon" measurements. *Atmos. Chem. Phys* **13**: 8365–8379. doi:10.5194/acp-13-8365-2013

Polissar AV, Hopke PK, Harris JM. 2001. Source regions for atmospheric aerosol measured at Barrow, Alaska. *Environ. Sci. Technol* **35**: 4214–4226.

Quinn PK, Miller TL, Bates TS, Ogren JA, Andrews E, et al. 2002. A 3-year record of simultaneously measured aerosol chemical and optical properties at Barrow, Alaska. *J. Geophys. Res* **107**(D11): 4130. doi:10.1029/2001JD001248

Quinn PK, Shaw G, Andrews E, Dutton EG, Ruoho-Airola T, et al. 2007. Arctic haze: current trends and knowledge gaps. *Tellus B* **59**: 99–114.

Raatz WE. 1989. An anticyclone point of view on low-level tropospheric long-range transport. *Atmos. Environ* **23**: 2501–2504.

Ramanathan V, Carmichael G. 2008. Global and regional climate changes due to black carbon. *Nat. Geosci* **1**: 221–227. doi:10.1038/ngeo156

Randel WJ, Wu F, Vömel H, Nedoluha GE, Forster P. 2006. Decreases in stratospheric water vapor after 2001: Links to changes in the tropical tropopause and the Brewer-Dobson circulation. *J. Geophys. Res* **111**: D12312. doi:10.1029/2005JD006744

Saha A, O'neill NT, Eloranta E, Stone RS, Eck TF, et al. 2010. Pan-Arctic sunphotometry during the ARCTAS-A campaign of April 2008. *Geophys. Res. Lett* **37**: L05803. doi:10.1029/2009GL041375

Sand M, Berntsen TK, Kay JE, Lamarque JF, Seland O, et al. 2013. The Arctic Response To Remote And Local Forcing Of Black Carbon. *Atmos. Chem. Phys* **13**: 211–224. doi:10.5194/Acp-13-211-2013

Schnell RC. 1984. Arctic haze and the Arctic Gas and Aerosol Sampling Program (AGASP). *Geophys. Res. Lett* **11**(5): 361–364.

Schnell RC, Watson TB, Bodhaine BA. 1989. NOAA WP-3D instrumentation and flight operations on AGASP-II. *J. Atmos. Chem* **9**: 1–16.

Schwarz JP, Gao RS, Fahey DW, Thomson DS, Watts LA, et al. 2006. Single-particle measurements of midlatitude black carbon and light-scattering aerosols from the boundary layer to the lower stratosphere. *J. Geophys. Res* **111**: D16207. doi:10.1029/2006JD007076

Sharma S, Brook JR, Cachier H, Chow J, Gaudenzi A, et al. 2002. Light absorption and thermal measurements of black carbon in different regions of Canada. *J. Geophys. Res* **107**(D24): 4771. doi:10.1029/2002JD002496

Sharma S, Lavoué D, Cachier H, Barrie LA, Gong SL. 2004. Long-term trends of the black carbon concentrations in the Canadian Arctic. *J. Geophys. Res* **109**: D15203. doi:10.1029/2003JD004331

Sharma S, Andrews E, Barrie LA, Ogren JA, Lavoué D. 2006. Variations and sources of the equivalent black carbon in the high Arctic revealed by long-term observations at Alert and Barrow: 1989–2003. *J. Geophys. Res* **111**: D14208. doi:10.1029/2005JD006581

Sharma S, Ishizawa M, Chan D, Lavoué D, Andrews E, et al. 2013. 16-year simulation of Arctic black carbon: Transport, source contribution, and sensitivity analysis on deposition. *J. Geophys. Res. Atmos* **118**: 943–964. doi:10.1029/2012JD017774

Shaw GE. 1983. Evidence for a central Eurasian source area of Arctic haze in Alaska. *Nature* **299**: 815–818.

Shaw GE. 1995. The Arctic haze phenomenon. *Bull. Am. Met. Soc* **76**: 2403–2413.

Shaw GE, Stamnes K. 1980. Arctic Haze: Perturbation of the Polar Radiation Budget. *Am. N.Y. Acad. Sci* **338**: 533–540.

Shindell D, Faluvegi G. 2009. Climate response to regional radiative forcing during the twentieth century. *Nat. Geosci* **2**: 294–300. doi:10.1038/ngeo473

Shindell D, Schulz M, Ming Y, Takemura T, Faluvegi G, et al. 2010. Spatial scales of climate response to inhomogeneous radiative forcing. *J. Geophys. Res* **115**: D19110. doi:10.1029/2010JD014108

Skouratov S. 1997. Vertical profiles of arctic haze aerosol in spring 1994 obtained by using spectrophotometric measurements *Atmos. Res* **44**(1–2): 113–124.

Solomon S, Daniel JS, Neely RR, Vernier JP, Dutton EG, et al. 2011. The persistently variable "background" stratospheric aerosol layer and global climate change. *Science* **333**(6044): 866–870. doi:10.1126/science.1206027

Stock M, Ritter C, Herber A, von Hoyningen-Huene W, Baibakov K, et al. 2011. Springtime Arctic aerosol: Smoke versus Haze, a case study for March 2008. *Atmos. Env* **52**: 48–55. doi: 10.1016/j.atmosenv.2011.06.051

Stohl A, Andrews E, Burkhart JF, Forster C, Herber A, et al. 2006. Pan-Arctic enhancements of light absorbing aerosol concentrations due to North American boreal forest fires during summer 2004. *J. Geophys. Res* **111**: D22214. doi:10.1029/2006JD007216

Stohl A, Klimont Z, Eckhardt S, Kupiainen K. 2013. Black carbon in the Arctic: the underestimated role of gas flaring and residential combustion emissions. *Atmos. Chem. Phys* **13**: 8833–8855. doi:10.5194/acp-13-8833-2013, 2013

Stone RS, Key JR, Dutton EG. 1993. Properties and decay of stratospheric aerosols in the Arctic following the 1991 eruptions of Mount Pinatubo. *Geophys. Res. Lett* **20**(21): 2359–2362.

Stone R, Mefford T, Dutton E, Longenecker D, Halter B, et al. 1996. *Barrow, Alaska, Surface radiation and meteorological measurements: January 1992 to December 1994*. NOAA Data Rep. ERL CMDL-11. Boulder, CO: US Department of Commerce: 81 pp.

Stone RS. 2002. Monitoring aerosol optical depth at Barrow, Alaska and South Pole; Historical overview, recent results, and future goals, in Colacino M, ed., *Proceedings of the 9th Workshop Italian Research on Antarctic Atmosphere, Rome, Italy, 22–24 October 2001*. Bologna, Italy: Ital. Phys. Soc: pp. 123–144.

Stone RS, Dutton EG, Harris JM, Longenecker D. 2002. Earlier spring snowmelt in northern Alaska as an indicator of climate change *J. Geophys. Res* **107**(D10): 4089. doi:10.1029/2000JD000286

Stone R, Douglas D, Belchansky G, Drobot S. 2005. Correlated declines in Pacific Arctic snow and sea ice cover. *Arc. Res. U S* **19**: 18–25.

Stone RS, Anderson GP, Andrews E, Dutton EG, Shettle EP, et al. 2007. Incursions and radiative impact of Asian dust in northern Alaska. *Geophys. Res. Lett* **34**: L14815. doi:10.1029/2007GL029878

Stone RS, Anderson GP, Shettle EP, Andrews E, Loukachine K, et al. 2008. Radiative impact of boreal smoke in the Arctic: Observed and modeled. *J. Geophys. Res* **113**: D14S16. doi:10.1029/2007JD009657

Stone RS, Herber A, Vitale V, Mazzola M, Lupi A, et al. 2010. A three-dimensional characterization of Arctic aerosols from airborne Sun photometer observations: PAM-ARCMIP, April 2009. *J. Geophys. Res* **115**: D13203. doi:10.1029/2009JD013605

Stroeve J, Serreze M, Holland M, Kay J, Maslanik J, et al. 2011. The Arctic's rapidly shrinking sea ice cover: A research synthesis. *Climatic Change* **110**(3–4): 1005–1027. doi:10.1007/s10584-011-0101-1

Tomasi C, Lupi A, Mazzola M, Stone R, Dutton E, et al. 2012. An update on Polar aerosol optical properties using POLAR-AOD and other measurements performed during the International Polar Year. *Atmos. Environ* **52**: 29–47.

Tomasi C, et al. 2014. Aerosol remote sensing in polar regions. *Earth-Science Reviews*, under review.

Thomason LW, Herber AB, Yamanouchi T, Sato K. 2003. Arctic Study on Tropospheric Aerosol and Radiation: Comparison of tropospheric aerosol extinction profiles measured by airborne photometer and SAGE II. *Geophys. Res. Lett* **30**(6): 1328: doi:10.1029/2002GL016453

Treffeisen R, Turnved P, Ström J, Herber A, Bareiss J, et al. 2007. Arctic smoke – aerosol characteristics during a record air pollution event in the European Arctic and its radiative impact. *Atmos. Chem. Phys* **7**: 3035–3053. doi:10.5194/acp-7-3035-2007

Twomey S. 1977. The influence of pollution on the shortwave albedo of clouds. *J. Atmos. Sci* **34**: 1149–1152.

UNEP. 2011. Near-term Climate Protection and Clean Air Benefits: Actions for Controlling Short-Lived Climate Forcers. Nairobi, Kenya: United Nations Environment Programme (UNEP): 78 pp.

Vernier J-P, Thomason LW, Pommereau J-P, Bourassa A, Pelon J, et al. 2011. Major influence of tropical volcanic eruptions on the stratospheric aerosol layer during the last decade. *Geophys. Res. Lett* **38**: L12807. doi:10.1029/2011GL047563

Warneke C, Bahreini R, Brioude J, Brock CA, de Gouw JA, et al. 2009. Biomass burning in Siberia and Kazakhstan as an important source for haze over the Alaskan Arctic in April 2008. *Geophys. Res. Lett* **36**: L02813. doi:10.1029/2008GL036194

Warren SG, Wiscombe WJ. 1980. A model for the spectral albedo of snow. II: Snow containing atmospheric aerosols. *J. Atmos. Sci* **37**: 2734–2745.

Yamanouchi T, Treffeisen R, Herber A, Shiobara M, Yamagata S, et al. 2005. Arctic Study of Tropospheric Aerosol and Radiation (ASTAR) 2000: Arctic haze case study. *Tellus B* **57**: 141–152.

Young CL, Sokolik IN, Dufek J. 2011. Regional radiative impact of volcanic aerosol from the 2009 eruption of Redoubt volcano. *Atmos. Chem. Phys. Discuss* **11**: 26691–26740. doi:10.5194/acpd-11-26691-2011

Contributions

- Contributed to conception and design: RSS, SS, AH, KE
- Contributed to acquisition of data: RSS, SS, SA, KE, DN
- Contributed to analysis and interpretation of data: RSS, SS, AH, KE, DN
- Drafted and/or revised the article: RSS, SS, AH, KE
- Approved the submitted version for publication: RSS, SS, AH, KE, DN

Acknowledgments

We are grateful to all field personnel who over the years have assured the continuity of quality data from BRW, ALT and NYA, and to flight crews of the Arctic aircraft missions. L. Barrie and F. Hopper initiated the BC measurement program at Alert. D. Longenecker provided assistance with data processing, J. Wendell with technical matters and P. Fukumura with calibration of NOAA photometers at Mauna Loa, HI. The NCEP gridded data were made available through the NOAA/ESRL Physical Sciences Division. A. Jefferson provided the NOAA EBC data from BRW. S. Yamagata provided the ASTAR 2000 EBC data, and H. Matsui and Y. Kondo the BC data from the 2008 ARCTAS campaign. S-M Li provided BC data derived from the SP2 used during 2009 and 2011 PAMARCMIP flights. We are also grateful to T. Grenfell, S. Warren and S. Doherty for sharing their insights regarding the darkening effect of BC in snow. M. Shepherd provided an earlier review of the manuscript. R. Stone dedicates his contribution to this study to his mentor, E. Dutton, who sadly passed away during preparation of this paper.

Funding information
The authors are grateful for support from their respective funding agencies. R. Stone received partial support from NSF with award ARC 11-07428, and from D. Winker through the NASA CALIPSO mission.

Competing interests
On behalf of all authors of this manuscript, I declare there are no conflicts of interest pertaining to any aspect of the study, be it financial, scientific or personal; RSS.

Supplemental material
Table S1. Appendix I. doi: 10.12952/journal.elementa.000027.s001

Data accessibility statement
Data, in the form of daily averages, used to generate the time series and monthly mean climatologies of AOD shown in Figures 2–4 are available from R. S. Stone by request. The aircraft data was assimilated with assistance from a number of contributors and will also be made available upon request with the express permission of those contributors. Additionally, all original raw photometric data is archived and is available upon request to NOAA/GMD.